Virtual and Biophysical Screening Targeting the γ-Tubulin Complex – A New Target for the Inhibition of Microtubule Nucleation

Olivier Cala, Marie-Hélène Remy, Valérie Guillet, Andreas Merdes, Lionel Mourey, Alain Milon, Georges Czaplicki

OPEN ACCESS Freely available online

PLOS ONE

Virtual and Biophysical Screening Targeting the γ-Tubulin Complex – A New Target for the Inhibition of Microtubule Nucleation

Olivier Cala[1,3], Marie-Hélène Remy[2,3], Valérie Guillet[1,3], Andreas Merdes[2,3], Lionel Mourey[1,3], Alain Milon[1,3], Georges Czaplicki[1,3]*

1 Institut de Pharmacologie et de Biologie Structurale, UMR 5089 CNRS – Université de Toulouse, UPS, Toulouse, France, **2** Centre de Biologie du Développement, CNRS, Toulouse, France, **3** Faculté des Sciences et de l'Ingénierie, Université de Toulouse, UPS, Toulouse, France

Abstract

Microtubules are the main constituents of mitotic spindles. They are nucleated in large amounts during spindle assembly, from multiprotein complexes containing γ-tubulin and associated γ-tubulin complex proteins (GCPs). With the aim of developing anti-cancer drugs targeting these nucleating complexes, we analyzed the interface between GCP4 and γ-tubulin proteins usually located in a multiprotein complex named γ-TuRC (γ-Tubulin Ring Complex). 10 ns molecular dynamics simulations were performed on the heterodimers to obtain a stable complex *in silico* and to analyze the residues involved in persistent protein-protein contacts, responsible for the stability of the complex. We demonstrated *in silico* the existence of a binding pocket at the interface between the two proteins upon complex formation. By combining virtual screening using a fragment-based approach and biophysical screening, we found several small molecules that bind specifically to this pocket. Sub-millimolar fragments have been experimentally characterized on recombinant proteins using differential scanning fluorimetry (DSF) for validation of these compounds as inhibitors. These results open a new avenue for drug development against microtubule-nucleating γ-tubulin complexes.

Citation: Cala O, Remy M-H, Guillet V, Merdes A, Mourey L, et al. (2013) Virtual and Biophysical Screening Targeting the γ-Tubulin Complex – A New Target for the Inhibition of Microtubule Nucleation. PLoS ONE 8(5): e63908. doi:10.1371/journal.pone.0063908

Editor: Alexandre G. de Brevern, UMR-S665, INSERM, Université Paris Diderot, INTS, France

Received September 24, 2012; **Accepted** April 8, 2013; **Published** May 15, 2013

Funding: This work was funded in part by 'Agence Nationale de la Recherche' ANR-08-BLAN-0281), and by a grant from 'Fondation RITC'. The funders had no role in study design, data collection and analysis, decision to publish, or preparation of the manuscript.

Competing Interests: The authors have declared that no competing interests exist.

* E-mail: Georges.Czaplicki@ipbs.fr

Introduction

Physiological or pathological processes are mainly controlled by protein–protein interactions (PPIs) [1,2], which constitute a promising but difficult pharmacological target in many diseases. Analysis of the interface between proteins might be of crucial interest in finding new binding sites and thus potential new drugs acting by complex destabilization. It has been shown that several residues of each protein are usually involved in the interaction. In the drug discovery process, two key issues have to be resolved: to determine a biological target and to characterize a therapeutic component, which binds to a specific binding site, capable of modulating the target activity. In the past decade, the fragment based lead discovery (FBLD) has emerged to help finding new drugs [3–5]. The first step in FBLD is to develop fragment libraries. They should be small and should respect physical properties according to the rules of five or of three [6,7]. These compounds can interact with the target with a weak affinity (high μM to mM range). The final step could be the combination of the best small elements in order to build a single molecular entity with affinity higher than that of the individual components.

This strategy offers possibilities of cancer chemotherapy, affecting microtubule dynamics and thus causing errors in the assembly of mitotic spindles, leading to cell cycle arrest [8]. Spindle microtubules in all eukaryotes are nucleated from multiprotein complexes. It was clearly shown that complexes of γ-tubulin are involved in microtubule nucleation [9–12]. An evolutionarily conserved heterotetramer forms the scaffold of this complex, composed of two copies of γ-tubulin and one of each of GCP2 and GCP3, called γ-tubulin small complex (γ-TuSC) [13]. In most eukaryotic cells, multiple γ-TuSCs associate with GCP4, GCP5 and GCP6 into a large complex of 2 MDa called γ-tubulin ring complex (γ-TuRC) [14,15]. Refined cryo-electron microscopy has revealed that the γ-TuRCs form short helical assemblies rather than 'rings' [16,17]. It is thought that the γ-TuRCs act as templates that nucleate the 13 tubulin protofilaments from dimers of α- and β-tubulin. These protofilaments establish lateral contacts to form the hollow microtubules [16].

Proteins of the GCP family show limited sequence homology [13,15]. Structural analysis of GCP4, combined with modeling, indicated that the core structure of all GCP family members is similar and that the GCP4 structure, as the prototype, can replace GCP2 or GCP3 in an EM density model of the γ-TuSC [18]. In addition, biochemical results show that GCP4 interacts with γ-tubulin via its C-terminal domain, as previously shown for GCP2 and GCP3 [18,19].

Several drugs such as paclitaxel derivatives and vinca alkaloids are now routinely used in chemotherapy of cancer, affecting dynamics of microtubules and thus provoking errors in mitotic spindle assembly. The targets of these inhibitors are α- and β-

tubulin [8]. So far no chemotherapeutic agents have been developed against γ-tubulin or against any of its associated γ-tubulin complex proteins except some drug-like compounds recently shown to interact with γ-tubulin [20]. Nevertheless, removal of γ-tubulin or of other γ-TuRC components from the cell induces changes in microtubule dynamics and spindle defects that resemble phenotypes obtained with microtubule drugs [21–23]. It will therefore be of major interest to investigate the assembly of γ-TuRCs, since these are crucial for microtubule assembly and may represent potential pharmacological targets: Whitehurst et al. [24] have described proteins of the γ-TuRC as putative targets whose depletion by siRNA sensitizes a lung cancer cell line at 1000-fold reduced doses of paclitaxel. Moreover, it has been shown that small amounts of siRNA against the γ-TuRC component NEDD1 potentiate the anti-mitotic activity of low doses of a Plk1 inhibitor [23].

In this study, we targeted the discovery of ligands that bind specifically at the interface of γ-tubulin and GCP4 proteins. This was possible thanks to the recently solved 3D structures of each of the proteins and the modeling of the γ-tubulin complex [18,25,26]. Biochemical interaction study of various GCP4 mutants selected from structure analysis highlighted residues involved in the interaction with γ-tubulin. Molecular dynamics simulations allowed obtaining a stable conformation of the complex in agreement with previous results of Kollman et al. [17]. We discovered a promising binding pocket at the interface between the two proteins and existing only after complex formation. This binding pocket has been used to find a potential inhibitor of this complex using FBLD. Sub-millimolar interaction has been demonstrated experimentally using differential scanning fluorimetry (DSF). These results are promising in search for new drugs that inhibit the interaction between GCP proteins and γ-tubulin and thus destabilize existing γ-TuRCs or prevent the assembly of its components. Since intact γ-TuRCs are essential for microtubule nucleation and mitosis, such drugs are expected to interfere with those mechanisms thus provoking mitotic spindle defects and arrest of the cell cycle.

Materials and Methods

Model Building of the GCP4-γ-tubulin Complex

The GCP4 crystal structure (PDB code 3RIP) was fitted into the yeast 8 Å cryo-electron microscopy (EM) reconstruction of the *Saccharomyces cerevisiae* γ–tubulin small complex (γ-TuSC) [18], along with the crystal structure of human γ-tubulin (PDB code 3CB2) already available. A pseudo-atomic model of the γ-TuSC was generated with GCP4 crystal structure as stands-in for yeast GCP2 and GCP3 (*S. cerevisiae* Spc97 and Spc98, respectively).

GCP4 fits remarkably well into the γ-TuSC cryo-EM structure. Some manual adjustments were necessary in the bend angle between the third and fourth helical bundles with relative rearrangements of N- and C-terminal domains. The obtained model revealed interaction surfaces between the complex components. Since some loops were missing in the original GCP4 crystal structure, they were added using the SuperLooper Web server [27]. Since the insertion of imported loop fragments may have induced a certain strain, a simulation of molecular dynamics has been used to allow the structure to relax and to adopt a preferential conformation in the complex. The details of the procedure are described in the next section.

Molecular Dynamics

The starting point for the MD simulations was the homology model of a GCP4-γ-tubulin tetramer [16–18]. Our objective was to verify the stability of the complex during a long MD run and to extract details on persistent intermolecular contacts from the MD trajectories.

The simulations were performed with the Amber9 software [28], using the all-atom ff03 force field [29] and the TIP3P water model [30]. A periodic system was created, containing the tetramer, 44 Na+ ions and 96432 water molecules, filling a box whose sizes were 138 × 143 × 176 Å in the X, Y and Z directions, respectively. The system minimization and the molecular dynamics simulations were performed using the parallel version of the PMEMD program. At first, the energy of the system was minimized by 200 cycles of the steepest descent (SD) algorithm, with the solute held fixed, by constraining its Cartesian coordinates using a harmonic potential with the force constant k equal to 500 kcal/mol/Å^2. In the second step, the energy was minimized by 200 cycles of SD and 1000 cycles of the conjugate gradients (CG) algorithm, with weakly restrained solute ($k = 10$ kcal/mol/Å^2). Next, a short 20 ps MD run was performed on weakly restrained solute ($k = 50$ kcal/mol/Å^2) with temperature varying linearly from 0 to 300 K. The temperature control was achieved using the Langevin dynamics with the collision frequency parameter γ equal to 1.0 ps^{-1}. The integration step used in this run was 1 fs. Throughout the calculations a cutoff of 12 Å was used for electrostatic interactions. The MD simulation continued for 180 ps at constant pressure of 1 bar and at 300 K with no restraints, with the integration step of 2 fs. The Langevin dynamics was used to control the temperature, with $\gamma = 1.0$ ps^{-1}, while the pressure was controlled by isotropic scaling with the pressure relaxation time $\tau_p = 2$ ps. Bonds involving hydrogen were constrained with the SHAKE algorithm. Finally, an MD simulation of 10 ns at constant pressure of 1 bar and at 300 K was launched, with atomic coordinates saved every 5 ps. The calculation was performed in parallel on two PowerEdge R410 servers, 16 cores in total, which worked at the speed of ca. 0.25 ns/day. Attempts to launch the calculation on more cores led to a slower computation, mainly due to the bottlenecks in the Gigabit Ethernet network.

Virtual Screening

Docking studies were performed using AutoDockTools [31] v1.5.4 and AutoDockVina [32]. The coordinate pdbqt file for γ-TuSC was prepared from the last frame of the molecular dynamics trajectory, using AutoDockTools v1.5.4. We used the last frame following a clustering analysis (*kclust* from the MMTSB toolset) of the last 2 ns of the trajectory, which showed that the frames formed only one single cluster with the dispersion of 1.5 Å with respect to the centroid. Since AutoDock Vina uses a united-atom scoring function, only polar hydrogens were retained, and partial charges were calculated for the protein according to the Kollman method. A grid box was built around the complex with the sizes of 120 Å, 82 Å and 70 Å in the x, y, and z dimensions, respectively. A spacing of 1 Å between the grid points was used, placing the interface of the chain B of GCP4 and the chain D of γ-tubulin to be at the center of the cube, i.e. x, y, and z offsets of −6.538 Å, 20.792 Å, and 28.966 Å, respectively. For the binding pocket, a grid box was built with x, y, and z sizes of 40 Å, 52 Å and 40 Å, respectively. A spacing of 1 Å between the grid points was used, placing the binding pocket to be the center of the cube, with x, y, and z centers at 19.821 Å, 28.209 Å, and 8.286 Å, respectively.

Fragments were provided by the Enamine chemical libraries. 50,000 molecules were sorted according to the rules of five of Lipinski to get 500 fragments in SD files. These files were translated to 3-dimensional coordinates in PDB format using Open Babel 2.2.3 [33]. Individual PDB files for each ligand were

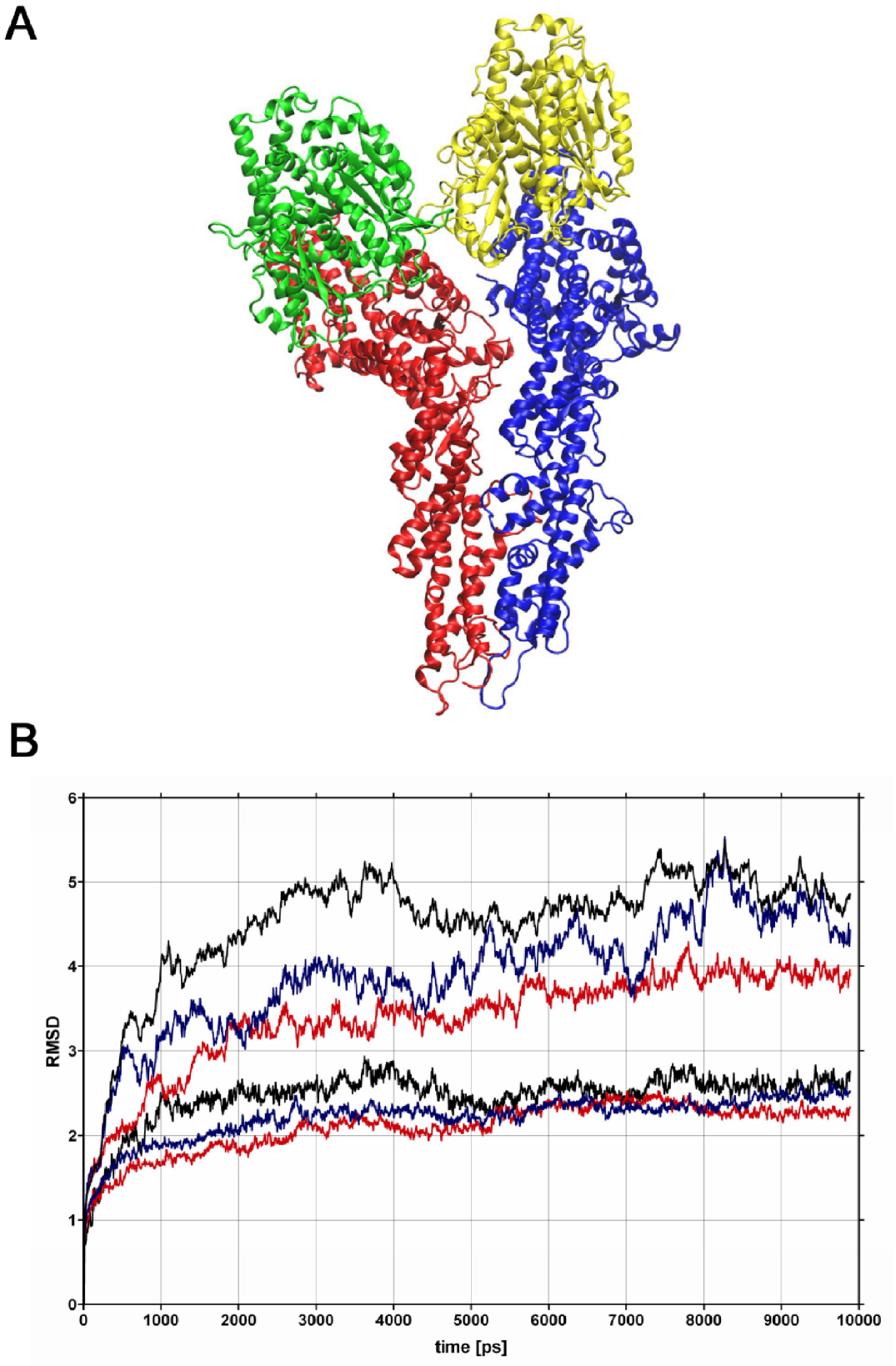

Figure 1. The (GCP4-γ-tubulin)$_2$ tetramer. (a) The starting structure of the tetramer. The four molecules are represented by different colors: dimer 1 with red (GCP4) and green (γ-tubulin), dimer 2 with blue (GCP4) and yellow (γ-tubulin). (b) RMSD of the atomic coordinates in the (GCP4-γ-tubulin)$_2$ tetramer as a function of time. Color coding: black for all atoms (upper trace) and for atoms from the intermolecular interface (lower trace), blue for dimer AC (upper trace GCP4, lower trace γ-tubulin), red for dimer BD (upper trace GCP4, lower trace γ- tubulin).
doi:10.1371/journal.pone.0063908.g001

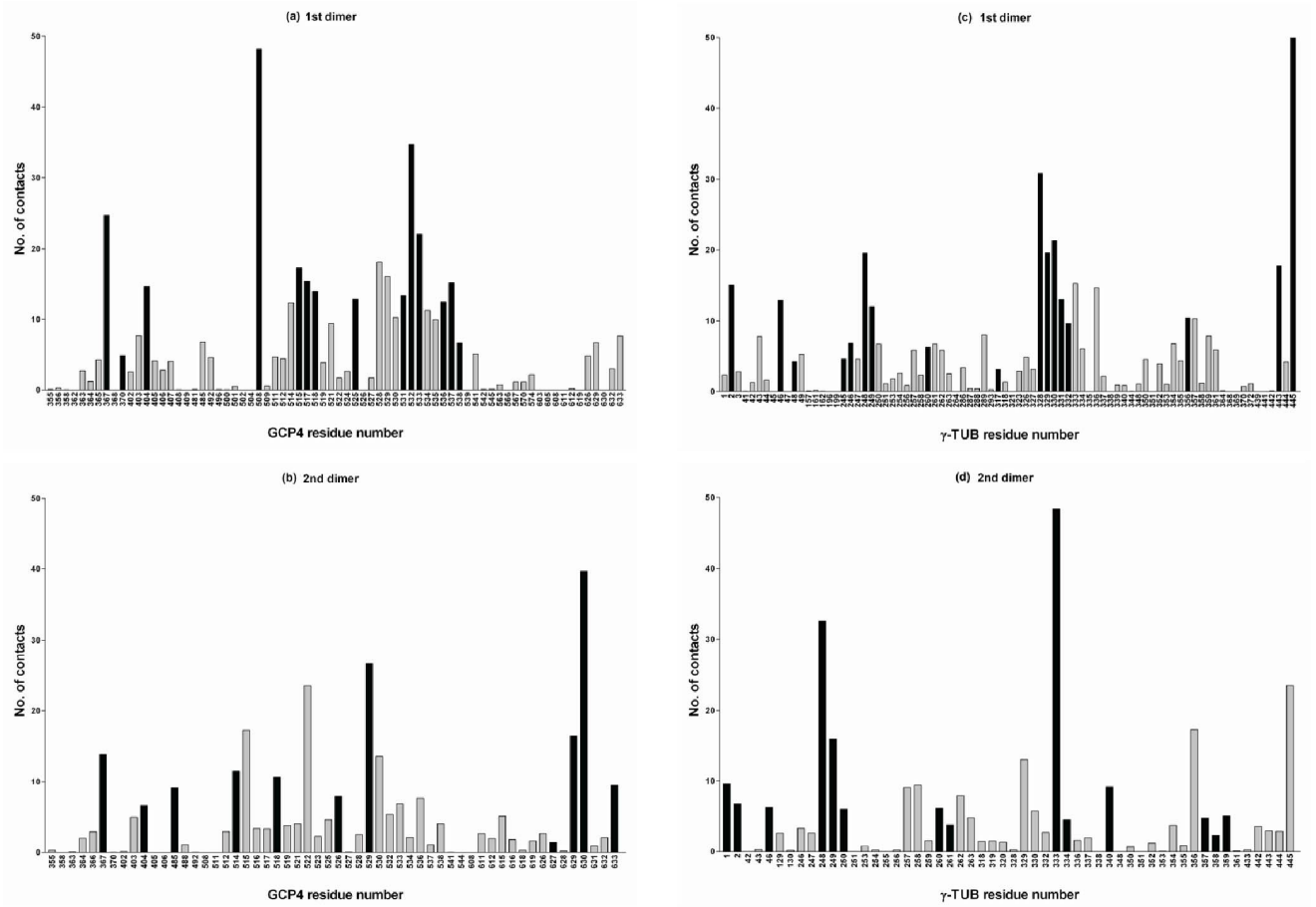

Figure 2. Histograms of contacts between two pairs of GCP4-γ-tubulin (γ-tub) molecules in a tetramer. Persistent contacts (valid in >90% of the MD trajectory frames) are in black. Data are for GCP4 molecules in the two dimers (A and B) and for the γ-tubulin molecules (C and D).
doi:10.1371/journal.pone.0063908.g002

prepared for docking using rigid and flexible side chains for amino acids involved in the pocket. Partial charges were computed according to the Gasteiger's method, non-polar hydrogens were merged and rotatable bonds were set using the prepare_ligand4.py script from MGLTools 1.5.4 [31].

A total of eight CPUs were used to perform the docking. Docking was carried out with the exhaustiveness value of 20 and the maximum output of 20 structures. For all other parameters we have used default values as defined by AutoDock Vina. The resulting conformations have been analyzed to find the most preferred ligands (clusters with a maximum number of conformations and minimum energy) in each case.

The resulting docking poses were visualized and overlaid with PyMol v0.99rc6.

The three-dimensional structure of GCP4 in one mutated form was generated by homology modeling, thus simulating the structural consequences of the S623R mutation on GCP4. For the evaluation of the results, the Deep-View analysis tool was used. (http://www.expasy.org/spdbv/, Swiss Institute of Bioinformatics, Geneva, Switzerland) [34]. Energy minimization was performed with the partial implementation of the GROMOS96 force-field using the steepest descent and conjugate gradient technique to correct the stereochemistry of the model.

Protein Expression and Purification

Expression of GCP4 and GCP4 S623R mutant was performed as described by Studier et al. [35]. BL21 (DE3) carrying a target plasmid was grown at 30°C with shaking at 190 rpm in LB medium supplemented with kanamycin at 100 µg/ml, and chloramphenicol at 25 µg/ml. The overnight cultures (10 mL) were collected by centrifugation when the optical density at 600 nm reached 0.8 and washed once with M9 medium without a carbon source. The washed bacteria were transferred to 1 L of M9 medium supplemented with 40 mL of carbon source 25X, 10 mL trace metals 100X, 1 mL vitamins mixed 1000X and kanamycin at 100 µg/ml final and grown at 20°C with agitation at 190 rpm for 3 days. Growth was monitored by measuring the optical density at 600 nm.

Purification of native and mutant proteins was carried out as described in Guillet et al. [18] at 4°C. Cells were resuspended in lysis buffer (50 mM sodium phosphate, pH 8.0, 300 mM NaCl, 10 mM imidazole, 5% glycerol) with a protease inhibitor cocktail, 2.5 mM tris-(2-carboxyethyl)phosphine (TCEP) and benzonase (5 U/mL culture) for 1 h and were lysed by sonication by applying five 30-s pulses. Cell debris was pelleted by centrifugation at 20,000 *g* for 40 min. The supernatant was diluted 1/5 in phosphate buffer (50 mM sodium phosphate, pH 8.0, 150 mM NaCl, 5% glycerol and 0.5 mM TCEP) supplemented with 10 mM imidazole and was then loaded onto a 5-ml HisTrap FF column (GE Healthcare). The column was washed first with

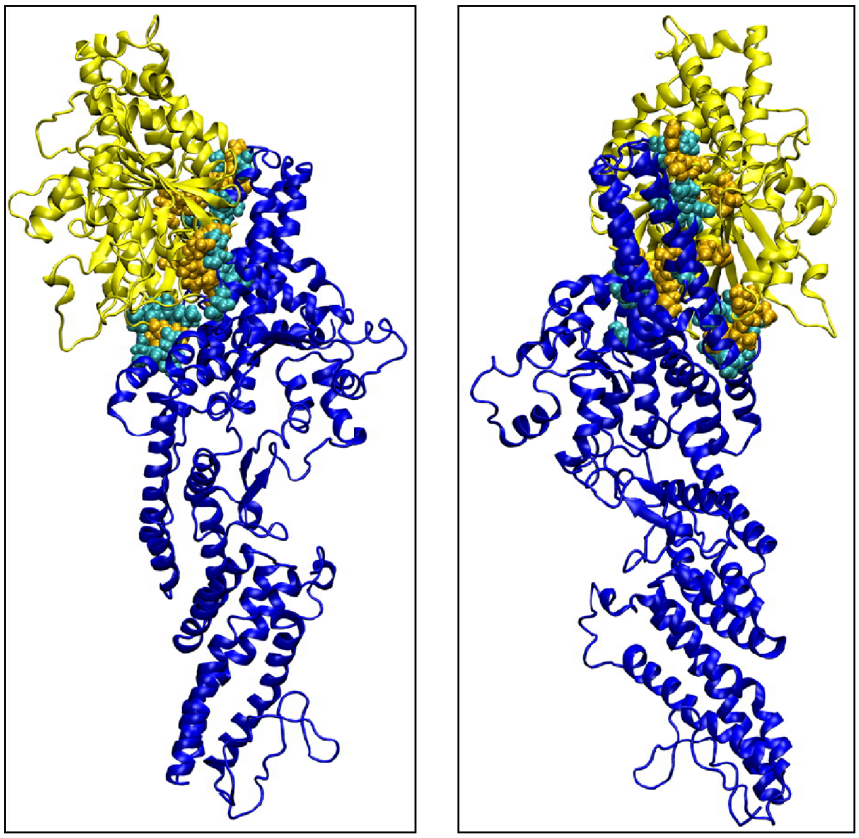

Figure 3. Persistent contacts between GCP4 (blue) and γ-tubulin (yellow) molecules. Two different views of the same dimer are shown. The residues involved in intermolecular contacts are highlighted in cyan (GCP4) and orange (γ-tubulin).
doi:10.1371/journal.pone.0063908.g003

phosphate buffer supplemented with 10 mM imidazole until the absorbance at 280 nm reached zero, then with 50 mM imidazole in phosphate buffer to nonspecifically elute proteins bound to the column. Recombinant proteins were eluted at 150 mM imidazole in phosphate buffer. The recombinant proteins were further purified by size-exclusion chromatography using a Superdex 200 16/60 column (GE Healthcare) equilibrated in gel filtration buffer (50 mM Tris, pH 8.2, 300 mM NaCl and 2 mM DTT).

The human *TUBG1* gene was inserted into a pET15b vector between the *XhoI* and *HindIII* restriction sites. The identity of the mutation and the correctness of gene insertion (location and orientation) were verified by DNA sequencing. The recombinant protein was expressed in *Escherichia coli BL21 (DE3)* host cells in LB medium supplemented with 100 µg/ml ampicillin. The cultures were grown at 25°C until OD600 reached a value of 0.8 and then induced with 1.0 mM IPTG for 18 h. Subsequently, the cells were harvested by centrifugation (7,000 rpm for 20 min in JS 7.5 rotor). The γ-tubulin protein was then isolated and purified from the inclusion bodies via refolding by dilution with immobilized metal ion affinity chromatography (IMAC) using a Ni-NTA column according to the protocol published by Friesen et al. [20]. The recombinant protein was further purified by size-exclusion chromatography using a Superdex 200 16/60 column (GE Healthcare), equilibrated in gel filtration buffer (50 mM Tris, pH 8.2, 300 mM NaCl and 2 mM DTT).

Differential Scanning Fluorimetry (DSF)

The DSF compound screen generally followed the protocol published by Niesen et al. [36]. Samples were loaded into a white/clear 96-well PCR plate (Bio-Rad) with each well containing a final volume of 20 µl. The concentration of protein in each well was 5 µM (0.4 mg/ml) for GCP4 or GCP4 S623R, 5 µM (0.27 mg/ml) for γ-tubulin in 50 mM Tris, pH 8.2, 300 mM NaCl, and 5X SYPRO Orange (Invitrogen). The purity of selected compounds from Enamine has been verified by NMR. They were used at a concentration from 1 µM to 1 mM. The PCR plates were sealed with optical quality sealing tape (Bio-Rad).

DSF experiments were carried out using a CFX96 real-time PCR system (Bio-Rad) set to use the 480/500 excitation and 560/580 emission filters. The samples were heated from 20 to 89.9°C at the rate of 6°C/min. A single fluorescence measurement was taken every 0.3°C. Melting temperatures were determined by performing a curve fit to the Boltzmann equation. The degree of thermal shift was calculated by comparing the melting temperature of the protein in each condition.

Results

Molecular Dynamics

The starting point for the molecular dynamics (MD) simulations was the homology model of the GCP4-γ-tubulin tetramer [16–18]. Our objective was to verify the stability of the complex during a long MD run and to extract details on persistent intermolecular contacts from the MD trajectory. On top of standard equilibrium parameters such as energy, volume, density and pressure of the system (data not shown), we followed the evolution of the root mean square deviation (RMSD) of the atomic coordinates of the whole system, as well as of its components. The system evolved in

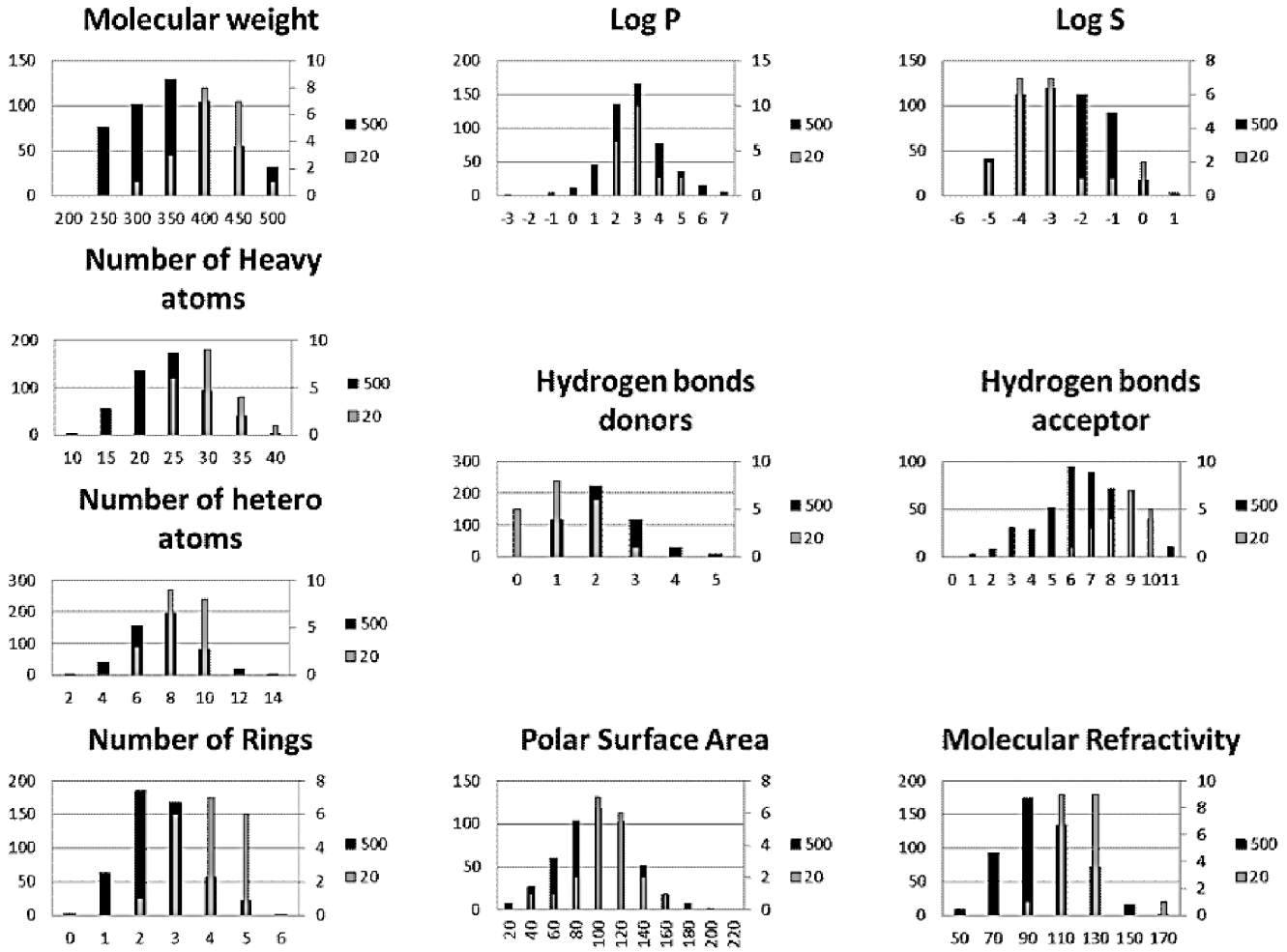

Figure 4. Molecular properties distribution of the fragments of the library used in this study. Molecular weight (MW), LogP, LogS, number of heavy atoms (HAC), hydrogen bonds donors (HD), hydrogen bonds acceptors (HA), number of hetero atoms (nHA), number of rings (NR), polar surface area (PSA) and molar refractivity (MR) of 500-fragment library (black bar chart) and 20-best-fragment library (grey bar chart). The table of the 500 fragments selected is given in supplementary material Figure S3.
doi:10.1371/journal.pone.0063908.g004

time from the initial, unoptimized model of the tetramer to the equilibrated and stable complex. Figure 1a shows the initial structure of the model, used as input in the MD simulation. Figure 1b shows the variation of RMSD of the system and its components as a function of time, calculated from a superposition of atomic coordinates for each frame of the trajectory with respect to the first of the saved frames (the first frame represents the complex before minimization and equilibration). The results have been corrected for the overall rotation and translation of the whole complex. It can be seen that the system needed ca. 3 ns to equilibrate. The remaining 7 ns were used for trajectory analysis.

To compute persistent intermolecular contacts at atomic level, we used in-house software, which analyzed trajectory frames (Figures 2 and 3). The program searched for distances between atoms belonging to different molecules below a specified threshold level in each frame. Since data obtained for several thresholds between 3 Å and 5 Å have given similar results, we have used the 3 Å threshold in the final analysis. For each distance found, its fluctuation was monitored across the trajectory to determine the percentage of total simulation time in which the contacts were present. If the percentage exceeded a predetermined threshold (90%), the contacts were reported as persistent. A histogram of interactions between pairs of molecules was created, providing detailed information on intermolecular interactions at atomic level. To double-check the results of our program, we used the Amber utility *ptraj*, which permits finding hydrogen bonds in the studied system. The Amber results represented a subset of our results, because hydrogen bonds are defined not only by the distances but also by the spatial positions of the atoms involved. Within each subset, the results were identical. The interface between the GCP4 and γ-tubulin molecules is described by two sets of amino acids, one for each dimer within the tetramer. The two lists of amino acids are close, but not identical: (i) Glu367, Gln370, Leu404, Gln508, Arg515, Arg517, Asn518, Asp525, Leu531, Gln532, Val533, Leu536, Glu537 and Ser538 for GCP4; Arg2, Arg46, Asp48, Pro245, Gly246, Met248, Asn249, Ile260, Ile317, Ile328, Ala329, Ile330, Leu331, Asn332, Gln356, Ile443 and Trp445 for γ-tubulin in the first dimer, and (ii) Glu367, Leu404, Arg485, Gln508, Trp514, Asn518, Asn526, Tyr529, Lys627, Leu629, Ser630 and Arg633 for GCP4 and Pro1, Arg2, Arg46, Met248, Asn249, Asn250, Ile260, Pro261, His333, Lys334, Arg340, Val357, Ala358 and Leu359 for γ-tubulin in the second dimer. As can be seen in Figure 2, the contacts in both dimers are not the same. This is mostly due to the fact that the interfacial

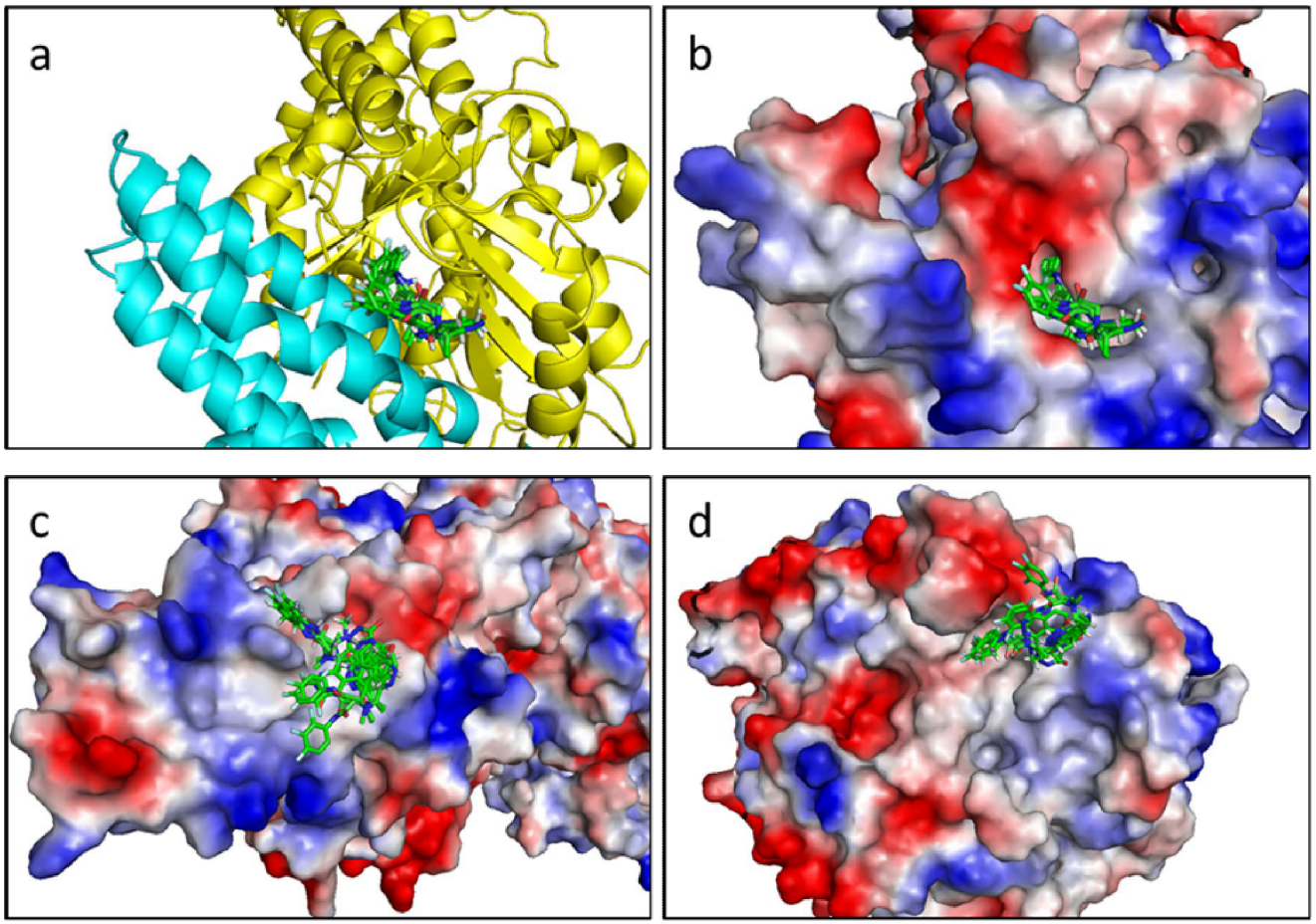

Figure 5. Superimposition of the 10 top positions of the best fragments. a. Cartoon representation of the binding site. b. Electrostatic surface representation of the binding site. c. Top view of the electrostatic surface representation of GCP4. d. Bottom view of the electrostatic surface representation of γ-tubulin.
doi:10.1371/journal.pone.0063908.g005

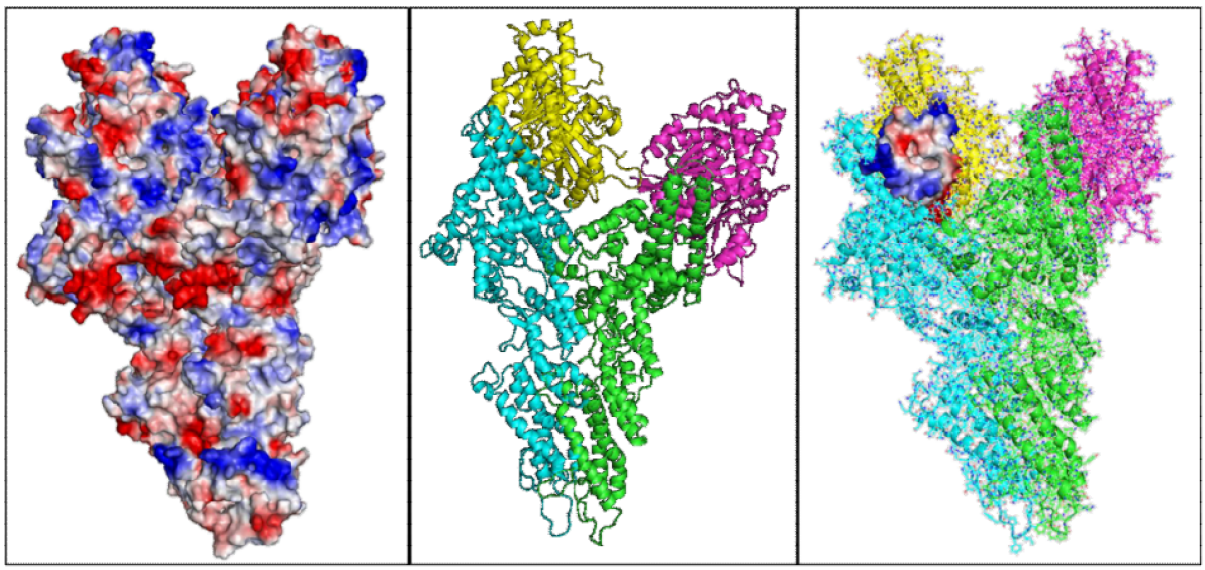

Figure 6. Binding site location. Electrostatic Surface (E.S.) representation of the γ-TuSC (left). Cartoon representation of the γ-TuSC (center) and E.S. representation of the binding pocket located within the γ-TuSC (right).
doi:10.1371/journal.pone.0063908.g006

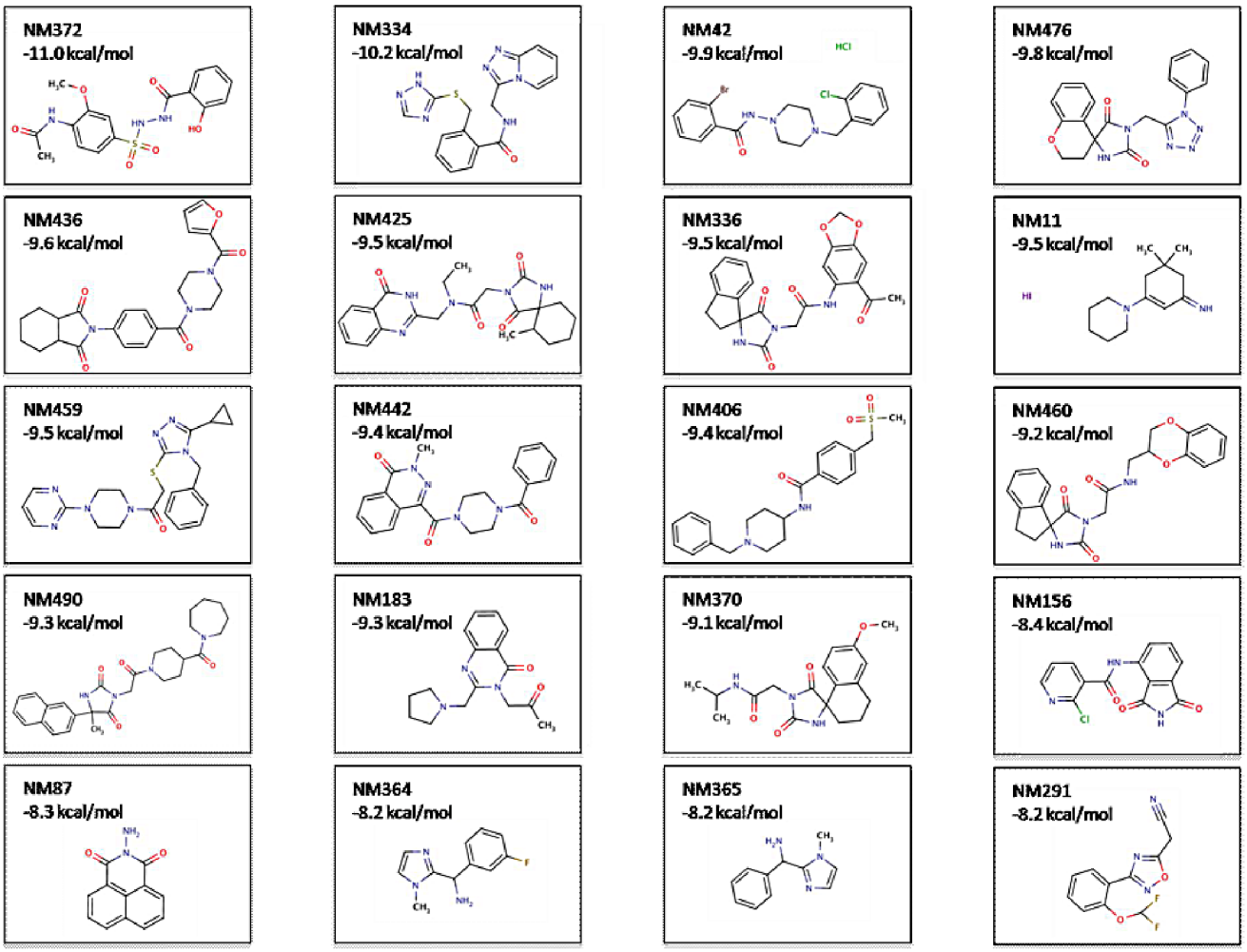

Figure 7. 20 best fragments from the virtual screening on the binding site. Molecules have been drawn with Marvin 5.11.3, 2012, ChemAxon (http://www.chemaxon.com). Carbon atoms, black; oxygen atoms, red; nitrogen atoms, blue; sulfur atoms, gold; chlorine atoms, green; fluorine atoms, light brown; bromine atoms, brown; iodine atoms, violet. The energy values correspond to the docking score.
doi:10.1371/journal.pone.0063908.g007

region is rich in flexible loops, whose extents are different in both dimers. For example, examination of the structure of the two contact regions reveals that the helix composed of 15 residues (328 to 342) in dimer BD is only 8 residues long (335 to 342) in dimer AC. Consequently, the RMSD differences between the atomic positions in the corresponding residues in the interface region are significant. However, the superposition of individual molecules (GCP4-A and GCP4-B, as well as γ-tubulin-C and γ-tubulin-D) does not indicate significant deviations (which amount to 6 Å for GCP4 and 3 Å for γ-tubulin).

Library Description

The fragment library was prepared from the set of Enamine compounds (www.enamine.net), characterized by physicochemical properties according to the rules of Lipinski [6,7]. Filters were applied for molecular weight from 200 to 500 Da, logP from −5 to 2, molar refractivity from 40 to 130 $m^3.mol^{-1}$, number of atoms from 20 to 70 (including H-bond donors [e.g.; OH and NH groups] and H-bond acceptors [e.g.; N and O atoms]), and polar surface area not greater than 200 $Å^2$ leading to 500 fragments.

Figure 4 shows the distribution of physicochemical properties such as molecular weight (MW), log P, log S, heavy atoms count (HAC), number of hetero-atoms (nHA), number of rings (NR), hydrogen bond donors (HD), hydrogen bond acceptors (HA), the polar surface area (PSA) and the molar refractivity (MR) for the total fragment library with the following average values: MW of 350 Da, logP of 3, logS of -3, PSA of 100 $Å^2$, MR of 90 $m^3.mol^{-1}$, and the average values of HAC, nHA, NR, HD and HA of 25, 8, 2, 2, 6, respectively.

Screening of the Fragments

The 500 members of our library were docked against the full γ-TuSC complex (dimer composed of GCP4 and γ-tubulin) derived from MD using Autodock Vina [32]. Next, the compounds were ranked based on their predicted binding energies and their maximum number of conformations. A large bounding box was used, which encompassed the entire γ-tubulin protein and the C-terminal region of GCP4. The results were processed by the built-in clustering analysis, and the lowest energy conformation from the largest cluster was selected as representative. Binding occurred in the same pocket, localized at the interface between GCP4 and γ-tubulin. It is notable that the same pocket exists on the other side of the γ-TuSC composed of GCP4 chain A and γ-tubulin chain C. The docking results in this area are equivalent to those obtained

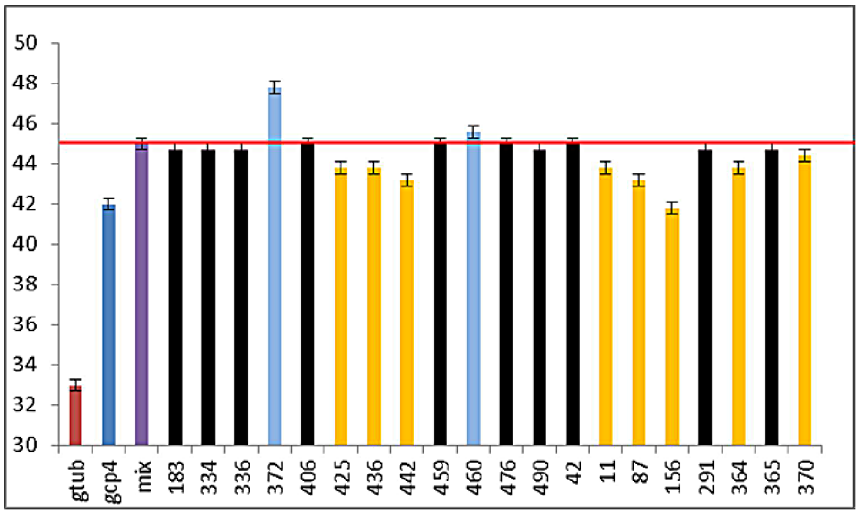

Figure 8. Graphical representation of T_m values determined by differential scanning fluorimetry. Melting temperatures (T_m) of the γ-tubulin-GCP4 complex with the 20 best fragments shown in Figure 7 (500 μM ligand concentration). T_m values for γ-tubulin (gtub) and GCP4 (gcp4) are in red and dark blue, respectively, whereas the T_m value for the GCP4-γ-tubulin complex (1:1) is in purple (mix). Black bars correspond to ligands whose addition had no effect on the complex; in orange, ligands showing a significant decrease of the T_m; in light blue, ligands showing a significant increase of the T_m. The red horizontal bar represents the T_m of the complex. Averages of triplicate data sets are shown. Error bars represent standard errors of the means.
doi:10.1371/journal.pone.0063908.g008

with chains B and D. Figure 5 shows the superimposition of ten poses of the best fragments in the binding pocket. The pocket, characterized below, was used for a second docking with the same 500-fragment library. The compound rankings were determined for each system. The twenty best molecules were recovered in the first thirty fragments of the 500-fragment library.

Binding Site Description

Using our 3D γ-TuSC model obtained from molecular dynamics simulations and according to the docking results, we focused our interest on the interface between the two proteins. All the molecules bind the complex in the same region localized on this interface, which allowed us to identify a pocket delineated by the two partners upon binding. This pocket only exists when GCP4 and γ-tubulin associate together. Interestingly, we showed that the region of GCP4 involved in the interaction with γ-tubulin is located on the C-terminal part of the protein between amino acids 349 and 637 (Figure S1. blue background). In regard to γ-tubulin, the C-terminal part is also involved in the interaction (Figure S1. green background). This is in excellent agreement with previous results based on fitting the crystal structure of GCP4 within the cryo-EM density map of γ-TuSC [18].

The pocket formed at the interface between γ-tubulin and GCP4 is composed of residues 246–264, 315–319, 337, 341, 347–358, 379–383, and 442–446 for γ-tubulin and 515–536 and 617–632 for GCP4 (Figure 6). All the lowest-energy positions of ligands obtained from virtual docking of the fragments to γ-TuSC are located within the pocket. Consequently, the refined screening procedures were focused on this binding pocket. By comparing the prediction of the binding site performed with Q-site Finder [37], we found that the best fragments were perfectly aligned with the predictive binding site (Figure S2).

Experimental Analysis by Differential Scanning Fluorimetry (DSF)

The twenty best compounds identified virtually after sorting on the number of conformations and the interaction energy (Figure 7), were then challenged in an effort to identify potentials inhibitors of γ-TuSC. A biophysical method, DSF [36], was used to identify compounds which alter the melting temperature (T_m) of the GCP4-γ-tubulin complex.

All the fragments were first tested on each protein alone and showed no effect (data not shown). γ-tubulin and GCP4 displayed T_m values of 33 and 42°C, respectively whereas a T_m of 45°C was found for the stoichiometric complex (Figure 8). This significant shift in melting temperature experimentally confirms that (i) there is formation of the complex composed of the two recombinant proteins *in vitro*, and (ii) that the complex is more stable than each of the two proteins alone. We thus confirmed *in vitro* that GCP4 can bind directly to γ-tubulin. Stable complexes of Flag-tagged γ-tubulin and V5-tagged GCP4 were isolated by immunoprecipitation with anti-Flag affinity beads as previously described [18]. Concerning the binding of the twenty best compounds identified from virtual screening of our library, ten of them (i.e. 50%) had effects on the T_m of the complex. Figure S4 shows the ^{1}H NMR spectra and structures of the four compounds producing the highest effect in DSF (ΔTm >2°C). The best hits could be separated in two categories where two compounds induced a stabilization of the complex whereas eight compounds induced a destabilization.

However, the fact that ligand binding affected the melting transition temperature of the complex did not guarantee that binding occurred in the expected binding pocket. In order to confirm this, and further confirm the predictive potency of our virtual docking procedure, we made a GCP4 mutant allowing the interaction with the γ-tubulin but blocking access to the pocket.

This mutant was obtained by replacing serine 623 of GCP4 by an arginine and showed a closed state of the binding pocket (Figure 9). Virtual docking with the mutant confirmed that our ligands were unable to bind to the complex in the mutated pocket. The compounds could be found all around the pocket and the binding energies increased from −11.0 kcal/mol for the wild type complex to −8.1 kcal/mol for the mutated complex. To confirm the existence of the binding pocket, expression and purification of

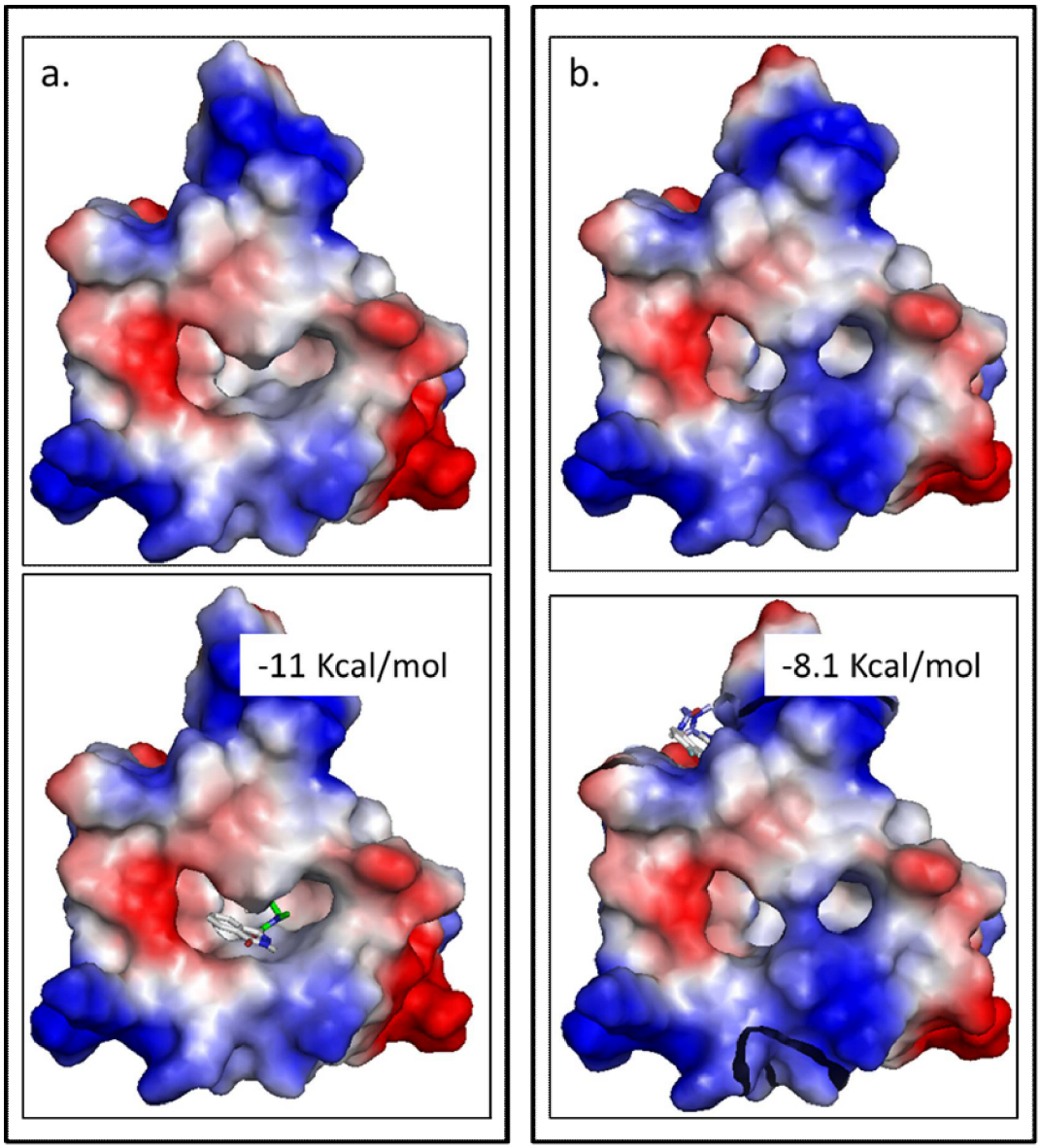

Figure 9. Mutation closing the binding pocket. a. Docking of the best compound, NM372, on the complex composed of GCP4 (WT) and γ-tubulin, without compound (above) and with compound (below). b. Docking of the best compound, NM372, on the complex composed of GCP4 (S623R) and γ-tubulin, without compound (above) and with compound (below). This figure clearly illustrates how the bulky and positively charged arginine side chain blocks the binding pocket.
doi:10.1371/journal.pone.0063908.g009

the GCP4 S623R protein was performed. Immunoprecipitation assays, performed as previously described [18] revealed that the GCP4 S623R retained the ability to bind directly to γ-tubulin as for the wild type protein.

The GCP4 S623R protein was also used in DSF experiment to validate the specificity of the binding site. The DSF results revealed that GCP4-S623R alone has a T_m of 51°C. The increase of T_m upon arginine introduction represents a stabilizing effect that has been observed for equivalent mutations in other proteins [38]. In complex with γ-tubulin, the T_m of the GCP4 mutant is increased to 54°C, showing a stabilization of the complex to the same extent as for the wild type complex, still confirming the interaction between γ-tubulin and the mutated GCP4.

The addition of the different compounds, even at a ligand concentration of 2 mM, showed no perturbation of the T_m. Thus, none of our ligands retained their capacity to bind to the complex when the access to the pocket binding site was prevented by an arginine. This in turns shows the specificity of the ligand-complex interaction towards the binding pocket identified by virtual screening.

Discussion

In this study, we propose a new target to inhibit microtubule assembly. Molecules currently used in cancer chemotherapy, such as paclitaxel and vinca alkaloids, target α/β-tubulin [20,39,40]. With the first three-dimensional structure of a γ-tubulin complex protein, GCP4 [18], and the proof of its interaction with γ-tubulin, we found it relevant to target the interface of this complex.

Our strategy was to identify and validate a binding site at the interface between GCP4 and γ-tubulin. We showed the existence of such a binding pocket at the interface of the two proteins and the specificity of the interaction of the best ligands from a designed fragment library in this pocket. Indeed, this binding pocket seemed to be a good target to find potential inhibitors of complex formation. Starting from a compound library of 50,000 fragments filtered according to physical properties and druggability, 500 small compounds were docked against the complex, targeting the binding pocket. The pocket is only created upon complex formation, so when the complex dissociates, the binding pocket no longer exists. We showed that some ligands can also bind to the C-terminal part of GCP4 after complex dissociation, but with a less favorable energy than the one obtained for the binding within the pocket of the complex.

The results obtained by virtual screening were confirmed by biophysical experiments. The twenty best hits identified by docking were used in DSF experiments and we showed that these compounds did not affect the T_m of GCP4 and γ-tubulin proteins alone but only induce a T_m shift on the GCP4- γ-tubulin complex. 50% of the chemicals induced an effect on this system either through stabilization or destabilization. Ligand-protein binding equilibrium usually leads to the stabilization of the system, and therefore to an increase of the melting temperature as visualized by DSF. Nevertheless, a number of cases have been experimentally observed where equilibrium-binding ligands destabilize proteins, thus decreasing the melting temperature of the system [41].

Using DSF experiments, we followed the unfolding of the protein. The T_m represents a transition where half of the protein concentration is folded and half is unfolded. According to Cimmperman [41], a ligand may bind to the native and/or unfolded protein. If the ligand binds to the unfolded state more strongly than to the native state, then the protein is destabilized by the ligand. On the other hand, if the ligand binds to the native form more strongly than to the unfolded state, then the protein is stabilized by the ligand. This means that some of our compounds bind to the unfolded state better than to the native state. Even if DSF experiments have been used to identify potential ligands, these compounds have to be validated as inhibitors, i) the dissociation constant seems to be around 500 μM but no titration had been done, ii) 500 μM is not enough to be considered as a specific inhibitor and has to be improved, and iii) DSF experiments only show that there is a binding but a structural study has to be performed to confirm the existence of the site and finally an *in vitro* assay has to be done to confirm the inhibition.

To prove the existence of the pocket, we prepared a variant of GCP4 where a single mutation could close the pocket. Indeed, we showed that the pocket could be closed by the single mutation S623R in GCP4 without disturbing its interaction with γ-tubulin. This also proves that the structural conformation of the complex has not been affected. Using virtual and biophysical screening, we showed that no binding could be observed between the previously studied ligands and the complex formed between S623R GCP4 and γ-tubulin.

It is known that defective γ-tubulin complexes lead to abnormalities in microtubule nucleation, and cause aberrant mitotic spindle assembly and cell cycle arrest [9,10,42–48]. In these previous studies, the assembly of γ-tubulin complexes was usually prevented by depleting essential components of the complex. Since we have shown here that small compounds from a chemical library bind to a hydrophobic pocket at the interface between GCP4 and γ-tubulin, the principal question arises whether such compounds can provoke a biological effect after the complex has already assembled in the cell. Provided that future optimization yields active cell-permeable compounds, we think that this should be possible, since we have successfully demonstrated that several of our compounds lower the melting temperature of the complex and should therefore destabilize existing complexes. Moreover, it is known from expression studies and biochemical analysis that assembly and disassembly of γ-tubulin complexes is a dynamic process [21,48], and that γ-tubulin complexes inside cells are in a dynamic exchange between an inactive cytoplasmic pool and an active pool bound to microtubule-organizing centers [49,50]. Consequently, the use of compounds that destabilize γ-tubulin complexes is expected to lower the amount of microtubule-nucleating γ-tubulin in the cell. Such reduced amounts of active γ-tubulin complexes will have an effect of microtubule dynamics, since reduced microtubule nucleation shifts the intracellular equilibrium between microtubule polymer and soluble dimer of α/β-tubulin, and since γ-tubulin complexes may directly affect the stability and dynamic properties of microtubules, in addition to their established role as microtubule nucleators [21,51–55]. As a combined effect, defective γ-tubulin complexes will lead to spindle defects and mitotic arrest, as previously documented by various groups [9,10,22,23,42–48].

Fragment-based lead discovery (FBLD) represents an excellent strategy to screen small and moderately complex molecules up to molecules with higher molecular weight and physical properties closer to drug-like compound [56,57]. This is because it has been recognized that fragment-like hit molecules can be efficiently developed and optimized toward leads. Several studies have shown that medicinal chemistry optimization of an already drug-like hit or a lead compound can result in a final compound with too high molecular weight and hydrophobicity. In this study, the compounds used were small molecules and displayed an observable effect at 500 μM concentration. The evolution of a lower molecular weight fragment hit represents an attractive alternative approach to optimization as it allows better control of compound properties. Computational chemistry can play an important role both prior to a fragment screen, in producing a target-focused fragment library, and after screening in the evolution of a fragment hit into a drug-like molecule.

In conclusion, we demonstrated that combining molecular dynamics, 3D structure analysis, virtual and biophysical screening was efficient in identifying γ-tubulin complex proteins as a new and very interesting target. Small molecule fragments were identified that bound to the complex composed of GCP4 and γ-tubulin, even though their binding might have been weak. Fragments represent a good tool to detect hot spots and identify new targets. Fragment-based hit identification also represents a powerful technique to build a new specific inhibitor of this binding site by either rational drug design or chemical optimization. Further characterization of the binding pocket and of small molecule inhibitors could represent a promising route for future cancer therapy.

Supporting Information

Figure S1 Sequence of the binding site. γ-tubulin at the top and GCP4 at the bottom. Residues of γ-tubulin and GCP4 involved in the interaction are shown on a green and blue background, respectively. Amino acids in red contribute to the binding pocket.
(DOCX)

Figure S2 Q-site finder binding site prediction. a. Cartoon representation of the binding site. GCP4 (green), γ-tubulin (cyan) and predicted binding site (magenta). b. Electro-

static surface representation of the binding site with the best fragment (green stick). c. Cartoon representation of the binding site with superimposition of the fragment in the predicted binding site. d. Electrostatic surface representation of the binding site with the best fragment superimposed to the predicted binding site.
(DOCX)

Figure S3 Molecular properties distribution of the 500 fragments. Molecular weight (MW), LogP, LogS, number of heavy atoms (HAC), hydrogen bonds donors (HD), hydrogen bonds acceptors (HA), number of hetero atoms (nHA), number of rings (NR), polar surface area (PSA) and molar refractivity (MR).
(DOCX)

Figure S4 NMR spectra of the best four hits. The effects of the best hits from docking on the melting temperature T_m of the complex are shown in Fig. 8 of the paper. This figure presents the NMR spectra for a subset of the ligands that had the most pronounced effect on the complex, i.e. whose T_m varied by at least 2°C. a. NM372. b. NM156. c. NM87. d. NM442. The 1D spectra have been acquired on a Bruker spectrometer operating at the proton frequency of 600 MHz, using a cryoprobe. Asterisks denote the solvent peaks: DMSO at 2.50 ppm and the residual HDO signal at 3.30 ppm. Molecules shown in insets have been drawn with Marvin 5.11.3, 2012, ChemAxon (http://www.chemaxon.com).
(DOCX)

Acknowledgments

Differential scanning fluorimetry experiments were carried out on a system which is part of the Integrated Screening Platform of Toulouse (PICT, IBiSA). This work was granted access to the HPC resources of CALMIP under the allocation 2012-[P1117]. The authors thank Dr. J.M. Kollman for making his high-resolution model of γ-TuSC available for this study. We acknowledge Drs Valentyna Semenchenko and Jack A. Tuszynski (University of Alberta, Edmonton, Canada) for kindly providing the plasmid and instructions to prepare γ-tubulin as well as Drs Michelle Moritz and David Agard (University of California, San Francisco, USA) for providing a batch of pure γ-tubulin protein, which was used in the early stages of the project.

Author Contributions

Conceived and designed the experiments: OC MHR VG GC. Performed the experiments: OC GC. Analyzed the data: OC MHR A. Milon A. Merdes GC. Contributed reagents/materials/analysis tools: OC MHR VG A. Milon LM A. Merdes GC. Wrote the paper: OC VG A. Milon LM A. Merdes GC.

References

1. Arkin MR, Wells JA (2004) Small-molecule inhibitors of protein-protein interactions: progressing towards the dream. Nat Rev Drug Discov 3: 301–317.
2. Pieraccini S, De Gonda R, Sironi M (2011) Molecular modeling of the inhibition of protein–protein interactions with small molecules: The IL2–IL2Rα case. Chemical Physics Letters 517: 217–222.
3. Barelier S, Krimm I (2011) Ligand specificity, privileged substructures and protein druggability from fragment-based screening. Curr Opin Chem Biol 15: 469–474.
4. Bottegoni G, Favia AD, Recanatini M, Cavalli A (2012) The role of fragment-based and computational methods in polypharmacology. Drug Discov Today 17: 23–34.
5. Hajduk PJ, Greer J (2007) A decade of fragment-based drug design: strategic advances and lessons learned. Nat Rev Drug Discov 6: 211–219.
6. Congreve M, Carr R, Murray C, Jhoti H (2003) A 'rule of three' for fragment-based lead discovery? Drug Discov Today 8: 876–877.
7. Lipinski CA, Lombardo F, Dominy BW, Feeney PJ (2012) Experimental and computational approaches to estimate solubility and permeability in drug discovery and development settings. Advanced Drug Delivery Reviews 64, Supplement: 4–17.
8. Jordan MA, Wilson L (2004) Microtubules as a target for anticancer drugs. Nat Rev Cancer 4: 253–265.
9. Joshi HC, Palacios MJ, McNamara L, Cleveland DW (1992) Gamma-tubulin is a centrosomal protein required for cell cycle-dependent microtubule nucleation. Nature 356: 80–83.
10. Oakley BR, Oakley CE, Yoon Y, Jung MK (1990) Gamma-tubulin is a component of the spindle pole body that is essential for microtubule function in Aspergillus nidulans. Cell 61: 1289–1301.
11. Oegema K, Wiese C, Martin OC, Milligan RA, Iwamatsu A, et al. (1999) Characterization of two related Drosophila gamma-tubulin complexes that differ in their ability to nucleate microtubules. J Cell Biol 144: 721–733.
12. Zheng Y, Wong ML, Alberts B, Mitchison T (1995) Nucleation of microtubule assembly by a gamma-tubulin-containing ring complex. Nature 378: 578–583.
13. Gunawardane RN, Martin OC, Cao K, Zhang L, Dej K, et al. (2000) Characterization and reconstitution of Drosophila gamma-tubulin ring complex subunits. J Cell Biol 151: 1513–1524.
14. Moritz M, Braunfeld MB, Sedat JW, Alberts B, Agard DA (1995) Microtubule nucleation by gamma-tubulin-containing rings in the centrosome. Nature 378: 638–640.
15. Murphy SM, Preble AM, Patel UK, O'Connell KL, Dias DP, et al. (2001) GCP5 and GCP6: two new members of the human gamma-tubulin complex. Mol Biol Cell 12: 3340–3352.
16. Kollman JM, Merdes A, Mourey L, Agard DA (2011) Microtubule nucleation by gamma-tubulin complexes. Nat Rev Mol Cell Biol 12: 709–721.
17. Kollman JM, Polka JK, Zelter A, Davis TN, Agard DA (2010) Microtubule nucleating gamma-TuSC assembles structures with 13-fold microtubule-like symmetry. Nature 466: 879–882.
18. Guillet V, Knibiehler M, Gregory-Pauron L, Remy MH, Chemin C, et al. (2011) Crystal structure of gamma-tubulin complex protein GCP4 provides insight into microtubule nucleation. Nat Struct Mol Biol 18: 915–919.
19. Kollman JM, Zelter A, Muller EG, Fox B, Rice LM, et al. (2008) The structure of the gamma-tubulin small complex: implications of its architecture and flexibility for microtubule nucleation. Mol Biol Cell 19: 207–215.
20. Friesen DE, Barakat KH, Semenchenko V, Perez-Pineiro R, Fenske BW, et al. (2012) Discovery of small molecule inhibitors that interact with gamma-tubulin. Chem Biol Drug Des 79: 639–652.
21. Bouissou A, Verollet C, Sousa A, Sampaio P, Wright M, et al. (2009) {gamma}-Tubulin ring complexes regulate microtubule plus end dynamics. J Cell Biol 187: 327–334.
22. Haren L, Remy MH, Bazin I, Callebaut I, Wright M, et al. (2006) NEDD1-dependent recruitment of the gamma-tubulin ring complex to the centrosome is necessary for centriole duplication and spindle assembly. J Cell Biol 172: 505–515.
23. Tillement V, Haren L, Roullet N, Etievant C, Merdes A (2009) The centrosome protein NEDD1 as a potential pharmacological target to induce cell cycle arrest. Mol Cancer 8: 10.
24. Whitehurst AW, Bodemann BO, Cardenas J, Ferguson D, Girard L, et al. (2007) Synthetic lethal screen identification of chemosensitizer loci in cancer cells. Nature 446: 815–819.
25. Aldaz H, Rice LM, Stearns T, Agard DA (2005) Insights into microtubule nucleation from the crystal structure of human gamma-tubulin. Nature 435: 523–527.
26. Rice LM, Montabana EA, Agard DA (2008) The lattice as allosteric effector: structural studies of alphabeta- and gamma-tubulin clarify the role of GTP in microtubule assembly. Proc Natl Acad Sci U S A 105: 5378–5383.
27. Hildebrand PW, Goede A, Bauer RA, Gruening B, Ismer J, et al. (2009) SuperLooper–a prediction server for the modeling of loops in globular and membrane proteins. Nucleic Acids Res 37: W571–574.
28. Case DA, Cheatham TE, 3rd, Darden T, Gohlke H, Luo R, et al. (2005) The Amber biomolecular simulation programs. Journal of computational chemistry 26: 1668–1688.
29. Ponder JW, Case DA (2003) Force fields for protein simulations. Advances in protein chemistry 66: 27–85.
30. Jorgensen WL, Madura JD (1983) Quantum and statistical mechanical studies of liquids. 25. Solvation and conformation of methanol in water. Journal of the American Chemical Society 105: 1407–1413.
31. Morris GM, Huey R, Lindstrom W, Sanner MF, Belew RK, et al. (2009) AutoDock4 and AutoDockTools4: Automated docking with selective receptor flexibility. J Comput Chem 30: 2785–2791.
32. Trott O, Olson AJ (2010) AutoDock Vina: improving the speed and accuracy of docking with a new scoring function, efficient optimization, and multithreading. J Comput Chem 31: 455–461.
33. Guha R, Howard MT, Hutchison GR, Murray-Rust P, Rzepa H, et al. (2006) The Blue Obelisk-interoperability in chemical informatics. J Chem Inf Model 46: 991–998.
34. Guex N, Peitsch MC (1997) SWISS-MODEL and the Swiss-PdbViewer: an environment for comparative protein modeling. Electrophoresis 18: 2714–2723.
35. Studier FW (2005) Protein production by auto-induction in high density shaking cultures. Protein Expr Purif 41: 207–234.

36. Niesen FH, Berglund H, Vedadi M (2007) The use of differential scanning fluorimetry to detect ligand interactions that promote protein stability. Nat Protoc 2: 2212–2221.
37. Laurie AT, Jackson RM (2005) Q-SiteFinder: an energy-based method for the prediction of protein-ligand binding sites. Bioinformatics 21: 1908–1916.
38. Strub C, Alies C, Lougarre A, Ladurantie C, Czaplicki J, et al. (2004) Mutation of exposed hydrophobic amino acids to arginine to increase protein stability. BMC Biochem 5: 9.
39. Dumontet C, Jordan MA (2010) Microtubule-binding agents: a dynamic field of cancer therapeutics. Nat Rev Drug Discov 9: 790–803.
40. Zhou J, Giannakakou P (2005) Targeting microtubules for cancer chemotherapy. Curr Med Chem Anticancer Agents 5: 65–71.
41. Cimmperman P, Baranauskiene L, Jachimoviciute S, Jachno J, Torresan J, et al. (2008) A quantitative model of thermal stabilization and destabilization of proteins by ligands. Biophys J 95: 3222–3231.
42. Barbosa V, Yamamoto RR, Henderson DS, Glover DM (2000) Mutation of a Drosophila gamma tubulin ring complex subunit encoded by discs degenerate-4 differentially disrupts centrosomal protein localization. Genes Dev 14: 3126–3139.
43. Colombie N, Verollet C, Sampaio P, Moisand A, Sunkel C, et al. (2006) The Drosophila gamma-tubulin small complex subunit Dgrip84 is required for structural and functional integrity of the spindle apparatus. Mol Biol Cell 17: 272–282.
44. Geissler S, Pereira G, Spang A, Knop M, Soues S, et al. (1996) The spindle pole body component Spc98p interacts with the gamma-tubulin-like Tub4p of Saccharomyces cerevisiae at the sites of microtubule attachment. Embo J 15: 3899–3911.
45. Hendrickson TW, Yao J, Bhadury S, Corbett AH, Joshi HC (2001) Conditional mutations in gamma-tubulin reveal its involvement in chromosome segregation and cytokinesis. Mol Biol Cell 12: 2469–2481.
46. Prigozhina NL, Oakley CE, Lewis AM, Nayak T, Osmani SA, et al. (2004) gamma-tubulin plays an essential role in the coordination of mitotic events. Mol Biol Cell 15: 1374–1386.
47. Sunkel CE, Gomes R, Sampaio P, Perdigao J, Gonzalez C (1995) Gamma-tubulin is required for the structure and function of the microtubule organizing centre in Drosophila neuroblasts. Embo J 14: 28–36.
48. Verollet C, Colombie N, Daubon T, Bourbon HM, Wright M, et al. (2006) Drosophila melanogaster gamma-TuRC is dispensable for targeting gamma-tubulin to the centrosome and microtubule nucleation. J Cell Biol 172: 517–528.
49. Khodjakov A, Rieder CL (1999) The sudden recruitment of gamma-tubulin to the centrosome at the onset of mitosis and its dynamic exchange throughout the cell cycle, do not require microtubules. J Cell Biol 146: 585–596.
50. Moudjou M, Bordes N, Paintrand M, Bornens M (1996) gamma-Tubulin in mammalian cells: the centrosomal and the cytosolic forms. J Cell Sci 109 (Pt 4): 875–887.
51. Cuschieri L, Miller R, Vogel J (2006) Gamma-tubulin is required for proper recruitment and assembly of Kar9-Bim1 complexes in budding yeast. Mol Biol Cell 17: 4420–4434.
52. Masuda H, Miyamoto R, Haraguchi T, Hiraoka Y (2006) The carboxy-terminus of Alp4 alters microtubule dynamics to induce oscillatory nuclear movement led by the spindle pole body in Schizosaccharomyces pombe. Genes Cells 11: 337–352.
53. Paluh JL, Nogales E, Oakley BR, McDonald K, Pidoux AL, et al. (2000) A mutation in gamma-tubulin alters microtubule dynamics and organization and is synthetically lethal with the kinesin-like protein pkl1p. Mol Biol Cell 11: 1225–1239.
54. Tange Y, Fujita A, Toda T, Niwa O (2004) Functional dissection of the gamma-tubulin complex by suppressor analysis of gtb1 and alp4 mutations in Schizosaccharomyces pombe. Genetics 167: 1095–1107.
55. Zimmerman S, Chang F (2005) Effects of gamma-tubulin complex proteins on microtubule nucleation and catastrophe in fission yeast. Mol Biol Cell 16: 2719–2733.
56. Law R, Barker O, Barker JJ, Hesterkamp T, Godemann R, et al. (2009) The multiple roles of computational chemistry in fragment-based drug design. J Comput Aided Mol Des 23: 459–473.
57. Wang YS, Strickland C, Voigt JH, Kennedy ME, Beyer BM, et al. (2010) Application of fragment-based NMR screening, X-ray crystallography, structure-based design, and focused chemical library design to identify novel microM leads for the development of nM BACE-1 (beta-site APP cleaving enzyme 1) inhibitors. J Med Chem 53: 942–950.

Figure S1 **Sequence of the binding site**. γ-tubulin at the top and GCP4 at the bottom. Residues of γ-tubulin and GCP4 involved in the interaction are shown on a green and blue background, respectively. Amino acids in red contribute to the binding pocket.

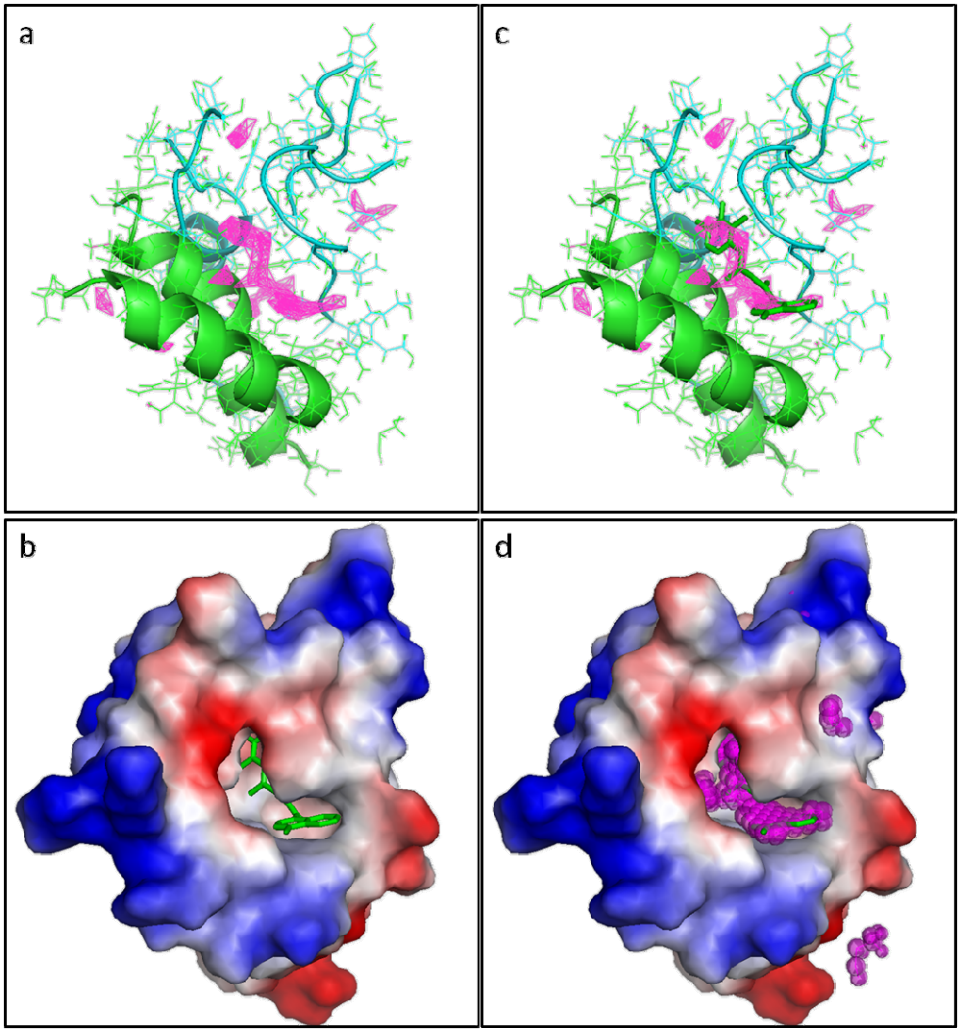

Figure S2 **Q-site finder binding site prediction**
a. Cartoon representation of the binding site. GCP4 (green), γ-tubulin (cyan) and predicted binding site (magenta). b. Electrostatic surface representation of the binding site with the best fragment (green stick). c. Cartoon representation of the binding site with superimposition of the fragment in the predicted binding site. d. Electrostatic surface representation of the binding site with the best fragment superimposed to the predicted binding site.

molecule	MW	LOGP	LOGS	HAC	HD	HA	nHA	NR	PSA	MR
1	247,245	-0,6293	-0.792	17	33	6.45	7	0	101,93	56,9555
2	258,768	3,8756	-4	16	31	2.25	5	2	63,21	70,8857
3	226,146	1,6975	-1.592	16	22	2.5	9	2	144,63	58,3394
4	258,314	0,8065	-0.753	18	40	6.5	6	1	76,66	65,6354
5	294,3	0,6671	-1.564	21	41	8	6	3	86,74	70,327
6	307,434	3,0073	-4.963	20	38	5.25	6	2	96,35	90,5587
7	310,369	2,0074	-3.998	21	40	7.9	7	2	100,91	81,4894
8	309,791	2,9823	-3.759	21	42	5	6	3	55,21	89,4687
9	499,324	1,099	-5.664	28	53	5.5	4	4	30,76	130,724
10	359,466	3,8326	-5.167	24	44	5.5	7	4	138,08	100,705
11	334,24	4,2318	-3.948	16	39	2	3	2	27,09	85,1767
12	326,35	1,6474	-2.659	24	44	9	7	3	85,46	91,5687
13	377,304	-0,1278	-4.495	19	48	2	3	3	17,07	89,0184
14	327,204	0,3215	-4.476	16	34	0.5	2	2	3,88	80,787
15	459,425	5,4263	-5.586	30	63	5.45	7	3	35,94	132,925
16	492,386	4,9598	-4.639	30	53	5.4	9	3	131,81	124,86
17	368,339	-0,105	-1.082	26	47	7.7	10	3	134,63	91,9063
18	310,35	2,78288	-4.666	23	43	6	6	3	83,96	86,998
19	232,067	-3,6889	0.002	7	12	2	5	0	80,29	42,7338
20	447,482	5,3979	-4.76	29	69	6.4	6	3	35,94	134,189
21	405,309	5,6573	-4.043	24	42	4.25	6	3	84,45	101,502
22	251,278	1,4571	-1.737	18	36	5.7	5	2	67,79	65,7717
23	305,371	2,7131	-1.905	19	35	9.25	8	2	106,3	70,1007
24	248,261	0,8008	-1.069	17	26	7	7	2	113,9	62,0432
25	318,25	-1,0817	-3.983	18	41	2.45	4	1	29,46	79,0462
26	458,492	4,8941	-5.255	33	55	9.5	10	5	117,07	126,064
27	302,371	1,6975	-3.193	22	45	7.7	6	2	78,99	89,5815
28	375,263	4,03538	-4.58	23	43	5.25	6	3	63,73	95,014
29	343,932	3,8061	-2.848	23	59	5.4	4	4	32,7	100,754
30	219,187	2,4107	-2.872	14	19	4	7	2	65,18	45,3787
31	219,187	2,4107	-2.872	14	19	4	7	2	65,18	45,3787
32	320,255	3,5515	-3.332	20	43	4.45	5	2	32,7	89,2238
33	370,283	0,9394	-5.604	23	44	2.5	3	3	20,95	101,079
34	493,977	-0,9995	-5.229	34	68	8.6	9	4	83,45	131,28
35	363,453	5,3647	-5.364	27	55	2.5	5	5	67,15	111,861
36	335,36	3,0724	-5.625	25	44	5	7	3	84,74	95,8262
37	403,273	3,79798	-4.406	25	46	6	7	4	72,96	99,392
38	393,923	4,3978	-4.711	27	57	5.4	5	3	32,7	113,025
39	364,667	0,6998	-4.709	21	37	2	5	3	42,79	93,1284
40	323,328	1,9267	-2.444	21	33	7.5	7	3	80,65	75,362

41	208,24	1,4752	-1.362	14	23	5	6	2	81,51	53,443
42	445,181	4,6338	-4.398	25	46	6	7	3	35,58	114,336
43	214,242	1,3512	-2.579	14	24	6	6	1	96,53	52,5132
44	291,344	1,4148	-1.804	18	32	8.2	8	2	120,53	69,1608
45	291,344	1,4148	-1.804	18	32	8.2	8	2	120,53	69,1608
46	301,303	2,3409	-2.822	20	34	8.5	6	3	106,92	83,7059
47	327,401	2,8001	-4.769	23	42	5.75	6	3	84,27	92,9337
48	469,328	-0,0469	-5.718	30	53	6.5	7	4	68,51	117,029
49	303,79	3,5119	-4.153	21	40	4.5	6	3	55,63	86,9567
50	232,987	-1,4366	-1.065	16	27	4.2	10	1	144,56	55,6562
51	389,942	5,2278	-4.429	26	51	5.5	6	3	73,47	111,948
52	345,443	2,8958	-4.992	23	40	7.25	8	3	124,21	97,8524
53	477,924	6,3858	-5.043	32	62	5.25	10	3	98,28	135,097
54	413,3	-0,2483	-5.346	22	47	5	6	3	52,85	104,72
55	324,259	3,9932	-2.441	19	42	3.5	4	3	20,54	88,543
56	221,133	0,9517	-2.209	15	21	5	7	1	59,3	43,5448
57	221,133	0,9517	-2.209	15	21	5	7	1	59,3	43,5448
58	396,994	-0,7271	-3.732	13	22	0.5	3	2	3,88	74,276
59	295,293	1,9983	-3.689	22	37	5	6	3	87,71	84,449
60	392,448	3,2497	-1.502	27	49	3.5	9	3	113,3	99,7528
61	239,291	2,5716	-2.381	16	30	5.75	5	2	63,78	63,0367
62	427,365	4,443	-2.411	28	57	6.95	7	4	49,08	125,268
63	310,372	1,0419	-2.728	21	39	7.2	8	2	119,14	86,7975
64	327,378	2,7783	-4.812	24	46	6.5	6	2	81,18	91,6572
65	456,945	3,6851	-5.114	31	55	8.75	9	5	95,39	131,471
66	349,226	2,8266	-3.531	21	39	5	6	3	61,12	91,0554
67	307,252	1,9317	-4.122	22	34	6.5	8	2	81,18	72,0272
68	377,236	3,1666	-2.064	23	41	5.75	7	3	86,03	94,1046
69	487,976	4,1204	-4.337	34	66	9.45	9	4	82,15	136,433
70	485,444	4,6011	-5.297	32	66	6.95	8	3	54,4	140,511
71	354,274	5,2128	-4.937	23	44	4.25	6	2	47,86	101,739
72	311,294	2,5733	-0.836	22	39	5	10	2	158,77	80,4323
73	434,361	4,3263	-3.717	28	57	8	10	3	84,64	127,182
74	302,276	2,0362	-4.044	20	30	5.5	9	2	85,11	66,7127
75	272,771	3,6187	-3.506	18	38	4	5	1	42,85	77,1097
76	444,956	4,9326	-4.876	32	60	7	6	5	49,33	137,356
77	303,383	1,6978	-3.249	21	40	7.2	7	3	101,29	87,3574
78	380,935	4,6266	-4.977	25	51	6.2	7	3	77,99	110,961
79	431,258	4,4844	-4.524	25	40	4	10	2	144,67	97,6076
80	335,186	2,7361	-2.046	21	37	6.75	9	2	84,89	93,456
81	274,189	2,5991	-1.264	17	34	5	5	2	18,84	82,611

82	308,635	3,2525	-1.892	18	34	5	6	2	18,84	87,621
83	497,54	3,1945	-5.85	36	69	6.5	10	4	138,17	139,535
84	360,676	2,4123	-4.385	24	33	8	11	2	94,07	74,9522
85	244,377	1,7077	-2.784	15	32	4	5	2	92,06	71,1507
86	201,677	2,6643	-2.208	12	20	3	5	1	82,17	54,0578
87	212,204	1,2477	-2.222	16	26	3.5	4	3	65,09	63,3124
88	367,398	2,8269	-4.965	27	50	7.25	7	3	74,49	103,455
89	315,281	1,0694	-1.668	23	38	8.5	8	3	99,64	76,4772
90	311,378	2,9963	-4.891	23	46	5.75	5	3	56,03	92,0167
91	355,817	2,9219	-4.092	24	46	6.75	8	2	74,61	92,0612
92	325,34	1,0569	-2.68	22	38	4.2	9	3	141,09	83,3796
93	383,398	2,7082	-4.152	28	50	4.2	8	3	132,64	105,134
94	383,326	-0,4435	-5.548	21	38	1.25	6	4	80,02	101,772
95	351,312	2,6814	-0.938	22	49	7.4	6	2	35,94	102,356
96	428,396	4,3738	-4.736	28	59	5.95	7	3	48,83	125,796
97	393,391	3,8411	-1.798	25	58	6.45	6	2	35,94	117,26
98	265,27	1,4189	-3.264	20	33	5.5	6	3	92,73	77,9756
99	265,27	1,4189	-3.264	20	33	5.5	6	3	92,73	77,9756
100	351,735	2,6861	-4.656	22	32	6.5	11	2	98	74,6457
101	372,888	4,2566	-3.499	26	53	5.75	5	4	32,78	113,692
102	261,75	4,1011	-3.441	18	34	3.5	4	2	37,28	78,4527
103	431,258	4,4844	-4.456	25	40	4	10	2	144,67	97,6076
104	290,813	2,0497	-1.301	18	37	6	7	2	76,32	78,516
105	299,836	3,1784	-2.63	20	46	5.4	4	2	32,7	88,5798
106	423,491	2,3427	-5.41	30	54	9.75	10	4	124,41	116,084
107	269,77	2,0414	-1.778	18	38	5.25	5	2	39,07	84,431
108	302,183	3,3903	-1.458	17	34	4	4	2	20,31	75,3655
109	314,851	4,3139	-2.896	21	47	4.75	5	1	50,36	90,6624
110	220,225	1,4074	-2.62	16	29	8	5	2	67,43	64,3124
111	220,225	1,4074	-2.62	16	29	8	5	2	67,43	64,3124
112	404,506	2,1109	-4.861	27	49	8.7	9	3	144,33	115,949
113	355,614	4,4683	-4.035	20	32	3.5	6	2	61,69	85,544
114	251,258	1,2208	-1.706	17	27	5.5	6	2	108,77	64,546
115	202,209	1,3251	-2.33	15	27	3.5	4	3	58,2	60,6724
116	202,209	1,3251	-2.33	15	27	3.5	4	3	58,2	60,6724
117	231,338	1,8557	-1.897	14	27	5.5	6	1	108,42	58,8257
118	212,249	1,8474	0.015	15	30	3.5	6	1	111,56	59,4596
119	243,218	2,4862	-2.584	18	28	2	6	3	95,91	70,4677
120	278,284	2,2875	-2.584	19	30	2	7	3	112,84	70,3089
121	249,262	1,6599	-3.468	18	34	5.25	5	2	64,63	65,6457
122	265,378	1,2753	-4.565	18	38	5	6	2	76,38	83,3057

123	226,726	2,7534	-3.972	14	26	1.5	4	2	49,69	67,6667
124	226,726	2,7534	-3.972	14	26	1.5	4	2	49,69	67,6667
125	252,763	2,6769	-4.443	16	30	1.5	4	3	45,53	73,577
126	363,878	4,1225	-4.726	25	52	4.7	5	3	50,72	101,766
127	302,759	3,0097	-3.207	21	37	4	6	3	70,67	82,9224
128	494,533	3,7119	-4.673	34	62	5.5	11	3	161,48	128,923
129	496,534	1,1984	-3.888	34	63	4.5	13	4	209,7	131,423
130	297,42	3,1081	-2.834	18	30	5.5	7	2	147,71	75,5524
131	277,728	2,1224	-1.984	17	29	7.5	8	1	100,88	62,7651
132	277,728	2,1224	-1.984	17	29	7.5	8	1	100,88	62,7651
133	397,319	5,1952	-5.296	25	44	3.5	7	3	69,42	104,884
134	260,292	1,2531	-2.868	19	36	5	6	2	92,91	75,5888
135	260,292	1,2531	-2.868	19	36	5	6	2	92,91	75,5888
136	423,506	3,2669	-2.854	28	51	9.7	10	3	134,85	111,422
137	225,264	2,2593	-0.541	15	27	5.5	5	2	85,61	54,7884
138	228,632	1,0287	-1.583	15	24	5.5	6	1	68,29	53,1422
139	308,353	0,6645	-2.94	21	38	7.5	7	2	107	88,464
140	308,353	0,6645	-2.94	21	38	7.5	7	2	107	88,464
141	431,509	1,7932	-4.184	30	57	8.7	10	3	154,54	119,096
142	341,313	0,5493	-2.354	24	43	8	9	1	109,39	80,7122
143	319,356	0,9719	-0.934	23	46	7.4	7	3	71,11	91,7442
144	253,278	1,3267	-2.793	17	29	5.75	7	2	103,71	63,7026
145	218,32	0,4665	-0.905	14	32	6.7	6	1	94,64	62,4538
146	301,297	0,7598	-2.786	22	39	6.5	7	3	90,29	78,6602
147	379,381	3,7172	-4.386	26	43	7.75	9	3	81,48	93,2867
148	365,378	2,7835	-3.198	26	49	3.5	8	2	118,23	93,4803
149	337,758	-0,5618	-4.621	23	39	4.75	8	2	88,03	89,9997
150	388,803	6,3466	-5.364	28	44	4	6	5	75,78	111,834
151	316,848	5,6056	-5.889	21	39	2	4	3	53,16	93,2737
152	365,338	3,1604	-1.793	23	52	6.45	6	2	35,94	107,922
153	208,118	-1,5656	-0.261	14	18	2.5	8	1	82,52	37,4999
154	232,235	0,80328	-1.658	17	29	6.5	5	1	70,4	59,9535
155	322,36	2,0079	-4.083	23	46	8	8	2	104,54	91,2854
156	301,685	2,2727	-3.247	21	31	5.5	7	3	88,16	78,8389
157	329,347	2,1462	-3.382	24	45	7.5	6	3	76,82	92,3095
158	351,227	3,3924	-4.393	21	34	5	9	2	99,01	83,4314
159	266,336	2,123	-3.401	19	42	5.5	5	2	66,48	79,4787
160	357,285	1,5523	-2.936	25	41	6.75	10	3	87,74	84,7134
161	307,775	2,24798	-1.505	21	40	7	6	3	48,73	88,868
162	356,374	2,876	-2.987	25	41	7.5	8	4	95,2	89,861
163	205,213	1,2943	-2.276	15	27	4	5	2	75,43	60,6221

164	205,213	1,2943	-2.276	15	27	4	5	2	75,43	60,6221
165	279,292	1,6445	-3.137	20	37	5.5	7	1	97,39	70,7889
166	326,345	-0,6797	-1.133	23	45	6.4	8	2	121,54	89,9112
167	292,332	2,5479	-2.546	20	34	5.5	7	2	99,1	75,2534
168	258,069	1,6544	-2.558	14	22	3.75	5	1	66,4	53,717
169	258,069	1,6544	-2.558	14	22	3.75	5	1	66,4	53,717
170	321,8	5,857	-5.513	23	42	1.5	3	5	26,03	96,7
171	412,414	3,7391	-4.047	28	48	5.5	11	2	163,13	102,892
172	403,858	6,2227	-5.65	29	51	3.25	5	6	40,58	114,197
173	317,366	2,1335	-2.893	22	39	7	8	3	110,62	81,8037
174	273,716	1,4147	-3.864	18	35	5.25	7	2	78,51	72,9154
175	273,716	1,4147	-3.864	18	35	5.25	7	2	78,51	72,9154
176	228,171	2,63058	-3.707	16	23	4	6	1	52,89	50,3127
177	228,171	2,63058	-3.707	16	23	4	6	1	52,89	50,3127
178	353,398	1,8531	-0.981	25	43	9	8	4	122,98	98,1254
179	495,056	6,0147	-5.133	35	73	8.5	7	5	67,23	145,114
180	316,44	3,0846	-2.587	20	41	7	7	2	103,1	83,5677
181	336,409	2,4252	-3.653	23	44	9	8	2	92,68	86,4172
182	395,816	1,4485	-1.739	25	42	8.5	12	1	161,49	89,442
183	285,341	1,5192	-0.708	21	42	8	5	3	55,2	85,97
184	421,535	3,1678	-3.719	31	64	9.25	7	3	71,3	124,789
185	397,424	1,8541	-3.935	29	54	8	8	3	88,18	112,903
186	236,267	1,0995	-1.027	17	33	5	5	1	67,43	62,9724
187	421,411	2,4408	-2.611	29	54	6	11	1	118,97	100,115
188	241,267	1,6047	-1.42	16	28	8.2	7	2	83,81	58,0727
189	241,267	1,6047	-1.42	16	28	8.2	7	2	83,81	58,0727
190	320,34	1,3293	-2.136	23	44	4.5	7	3	106,94	86,6303
191	363,388	3,0502	-4.431	25	43	3	9	3	153,79	93,6433
192	225,264	1,7355	-1.118	15	27	4.5	5	2	86,85	56,7474
193	325,359	1,7774	-4.486	22	39	6.5	8	2	103,81	89,3484
194	351,447	3,5899	-4.372	23	41	9	9	2	136,48	93,4651
195	432,553	4,3777	-3.738	31	68	4.5	7	3	106,94	120,454
196	401,456	1,4715	-0.586	29	57	7	8	3	101,39	118,784
197	444,564	3,6322	-3.197	32	70	5	7	4	98,15	127,316
198	385,414	2,9577	-4.145	28	52	8	8	2	105,76	105,376
199	252,742	0,5305	-1.945	14	23	5	7	1	106,8	63,8397
200	252,742	0,5305	-1.945	14	23	5	7	1	106,8	63,8397
201	250,277	0,8705	-3.218	17	28	6	7	2	105,12	64,6112
202	386,442	3,6898	-2.862	28	54	4	7	2	115,73	108,299
203	367,437	2,2336	-2.742	26	55	4.9	7	2	116,09	97,8431
204	242,745	3,0356	-1.941	16	34	4	4	1	41,13	70,2264

205	242,745	3,0356	-1.941	16	34	4	4	1	41,13	70,2264
206	363,679	5,2963	-4.298	21	39	1.5	4	4	27,82	96,7924
207	418,493	1,745	-3.227	28	48	10	11	3	180,51	110,206
208	261,276	0,4635	-2.263	19	35	6	6	2	69,72	75,5487
209	314,405	2,2713	-1.759	22	42	7.5	6	3	79,26	89,866
210	420,245	1,2004	-1.343	27	46	7.5	11	2	127,25	106,596
211	306,208	4,3681	-4.395	18	31	3	6	2	59,59	77,261
212	306,208	4,3681	-4.395	18	31	3	6	2	59,59	77,261
213	329,35	1,4336	-3.016	24	45	7	7	3	92,5	92,7703
214	480,594	2,8355	-3.527	34	75	6.65	9	3	128,56	132,946
215	350,413	0,4644	-1.651	25	53	9.5	8	3	90,03	105,868
216	481,519	2,7199	-2.687	33	60	9.75	12	2	161,93	121,85
217	323,387	2,5375	-2.06	23	48	5.25	7	1	102,68	87,1408
218	346,404	1,7046	-4.203	24	45	8.5	8	4	120,5	92,4597
219	361,267	5,7063	-4.102	21	32	6	8	3	95,68	88,7087
220	447,435	1,605	-3.395	32	58	7.45	10	3	151,62	111,983
221	278,33	1,6275	-3.134	19	34	6.25	7	2	94,34	73,3307
222	249,223	0,8319	-1.594	18	30	5.5	7	2	93,34	62,5494
223	327,373	1,5075	-2.173	23	47	3.95	7	1	116,09	86,2951
224	286,324	1,5887	-0.532	20	41	3	7	1	129,72	73,3837
225	268,312	2,2057	-1.573	17	27	6.5	7	3	118,76	62,924
226	460,305	3,0293	-4.541	30	53	5.2	10	2	116,53	112,49
227	290,357	1,9899	-1.776	21	44	6.25	5	2	72,63	84,1604
228	233,22	1,48078	-3.444	17	28	5	5	1	79,55	60,503
229	239,251	1,9958	-1.102	16	26	6.5	7	2	120,45	56,2424
230	313,311	0,8503	-3.265	23	40	8.75	8	3	91,04	84,6377
231	470,556	2,3554	-2.933	33	71	7.4	10	2	146,58	127,075
232	465,739	2,6932	-3.226	28	45	10	12	3	100,96	113,147
233	393,436	2,5927	-4.641	27	49	7.2	10	3	123,44	97,4114
234	331,646	3,7368	-1.298	18	31	6	8	2	57,79	82,3557
235	331,646	3,7368	-1.298	18	31	6	8	2	57,79	82,3557
236	234,683	2,6996	-1.673	13	17	6	7	2	96,54	50,498
237	234,683	2,6996	-1.673	13	17	6	7	2	96,54	50,498
238	264,234	1,2581	-3.134	19	32	6	7	2	90,54	65,6397
239	352,425	1,4168	-1.417	25	54	9.4	7	2	94,25	97,5062
240	204,182	0,4811	-1.45	15	24	6	5	2	72,19	53,8438
241	204,182	0,4811	-1.45	15	24	6	5	2	72,19	53,8438
242	401,494	1,8938	-2.687	28	64	6.6	8	3	125,32	103,183
243	362,334	1,9158	-2.891	26	45	9	9	2	116,1	89,8014
244	346,275	2,9796	-5.19	21	39	4.2	7	3	71,28	98,3037
245	309,285	1,6791	-2.772	21	39	6	9	1	78,51	75,2314

246	236,673	2,7121	-1.191	14	23	5.5	6	1	60,98	52,509
247	456,849	2,7954	-3.053	31	53	6	11	2	125,4	110,975
248	466,935	3,7245	-4.126	31	55	6.4	10	3	157,22	118,438
249	484,95	2,0722	-4.003	32	58	8.4	11	3	155,85	127,403
250	465,54	1,8114	-1.204	33	69	7.45	10	3	137,43	125,172
251	301,221	1,5354	-3.927	21	32	6	9	2	78,51	72,3804
252	267,324	0,7354	-1.166	19	42	7.2	6	3	61,88	80,5137
253	260,272	1,9399	-2.912	18	29	5.5	7	4	107,91	67,4494
254	303,826	4,7766	-4.007	21	43	2.25	3	2	21,26	90,9077
255	303,826	4,7766	-4.007	21	43	2.25	3	2	21,26	90,9077
256	396,463	2,6176	-4.414	28	51	6.5	8	4	113,75	114,576
257	205,236	1,8634	-2.038	14	22	5.5	5	2	83,12	54,1232
258	415,42	4,9307	-4.526	26	54	5.2	6	3	54,51	124,554
259	324,632	6,319	-5.999	20	33	1	4	3	12,89	89,13
260	439,461	1,5626	-3.933	32	60	9.7	9	4	97,41	125,403
261	340,871	2,8346	-5.191	22	43	5	7	2	91,15	103,828
262	303,399	2,4588	-1.715	22	48	7	5	2	75,43	92,0991
263	448,897	3,6008	-5.801	31	57	4.9	9	3	121,88	117,17
264	257,349	2,5078	-2.436	17	37	7	5	2	71,62	66,8017
265	306,852	3,9236	-2.245	19	41	6.5	6	1	57,79	81,1997
266	369,929	4,3652	-1.071	25	58	6.5	6	3	57,51	106,323
267	299,863	5,2399	-4.696	19	41	2	5	2	72,08	87,3314
268	299,863	5,2399	-4.696	19	41	2	5	2	72,08	87,3314
269	370,873	5,0211	-4.069	26	52	2.5	5	5	46,28	109,459
270	229,635	2,2786	-3.079	15	24	4.5	5	1	46,17	55,7032
271	229,635	2,2786	-3.079	15	24	4.5	5	1	46,17	55,7032
272	269,767	3,3206	-1.861	18	38	4.75	4	2	40,54	79,3225
273	269,767	3,3206	-1.861	18	38	4.75	4	2	40,54	79,3225
274	251,348	2,2723	-2.931	17	34	5	5	1	85,25	73,5361
275	272,306	0,3337	-0.82	20	38	8	7	3	67,15	80,421
276	284,31	2,3703	-2.594	21	38	6.75	5	2	68,29	78,0262
277	292,34	1,628	-2.825	19	29	8	9	3	138,61	72,3892
278	283,325	1,4149	-1.723	21	40	7	5	3	53,51	87,6805
279	372,461	1,9315	-3.287	27	57	9.45	7	3	68,5	110,001
280	261,252	1,2403	-3.898	19	32	4.5	6	2	63,99	67,2002
281	460,563	4,0043	-3.418	33	71	4.75	8	4	124,96	124,478
282	232,664	2,3006	-1.352	15	27	4.7	6	1	77,07	58,4789
283	232,664	2,3006	-1.352	15	27	4.7	6	1	77,07	58,4789
284	267,283	2,03938	-3.464	20	34	5.75	5	2	75,01	72,5467
285	232,278	1,7852	-2.385	17	34	4.25	4	2	58,2	64,5199
286	395,405	3,0811	-4.198	27	47	8.5	10	3	117,1	96,0109

287	217,242	2,1323	-1.49	14	25	6	6	1	87	50,4204
288	217,242	2,1323	-1.49	14	25	6	6	1	87	50,4204
289	375,373	2,5686	-3.214	27	49	3.75	8	3	114,32	96,2963
290	337,821	0,1553	-4.645	22	39	3.25	6	3	82,56	92,003
291	251,189	2,40408	-3.546	18	26	5	7	2	71,94	55,85
292	251,189	2,40408	-3.546	18	26	5	7	2	71,94	55,85
293	370,626	-0,5899	-4.319	21	34	4.5	6	2	47,25	84,581
294	365,491	0,2897	-4.803	16	28	0.5	4	2	3,88	78,746
295	301,364	2,747	-2.901	21	39	5.5	6	4	99,16	82,1934
296	327,373	2,1464	-2.74	23	47	3.95	7	1	105,09	85,9003
297	327,334	4,1529	-3.648	22	36	7	8	2	93,54	79,2744
298	300,332	2,5376	-2.965	21	35	6.75	6	3	88,91	80,5125
299	364,371	1,5423	-3.77	26	48	8.7	9	2	110,42	96,3756
300	433,477	1,3739	-4.316	31	61	9.2	10	3	111,59	119,099
301	376,447	2,896	-4.094	27	55	3.2	7	2	100,79	103,624
302	324,349	2,7745	-4.947	22	38	5.5	8	3	85,11	79,2207
303	312,365	3,5105	-3.133	20	33	10	8	2	135,11	76,0196
304	351,785	1,1704	-2.613	24	44	8.2	8	3	78,95	97,7487
305	384,452	3,2298	-2.233	27	49	8	8	3	115,32	102,021
306	268,289	0,938	0.098	18	31	8	7	2	83,14	67,1375
307	331,406	3,1474	-3.177	24	51	1.5	5	4	86,63	91,2093
308	293,365	2,5445	-3.319	19	31	7.5	7	2	125,49	75,6582
309	296,276	1,0776	-1.624	21	37	7.5	8	1	116,95	72,7326
310	425,481	2,4074	-5.795	31	61	9.25	9	4	105,44	123,959
311	267,776	2,9398	-1.321	16	33	5	7	1	74,44	65,8957
312	267,776	2,9398	-1.321	16	33	5	7	1	74,44	65,8957
313	326,865	-1,84482	-2.187	22	50	6	6	3	56,13	96,0047
314	374,391	0,5711	-3.059	27	52	10	9	4	103,17	108,421
315	312,32	2,8355	-3.626	23	41	6.7	6	3	77,61	83,3328
316	243,756	3,7308	-3.401	15	29	2	5	2	72,08	68,1034
317	243,756	3,7308	-3.401	15	29	2	5	2	72,08	68,1034
318	254,756	2,8241	-0.851	17	36	4	4	2	41,13	74,8194
319	254,756	2,8241	-0.851	17	36	4	4	2	41,13	74,8194
320	343,354	1,2358	-4.319	24	39	5.5	7	3	120,77	90,2172
321	422,3	3,592	-4.387	27	52	3.95	9	2	116,09	103,338
322	286,309	1,5647	-2.796	20	32	8	7	3	105,12	76,7707
323	344,365	0,7236	-4.122	25	47	7.5	8	3	84,74	99,4835
324	480,488	2,8859	-4.429	35	64	9.5	10	5	93,11	135,779
325	403,426	2,2034	-3.358	29	54	5.95	8	2	133,16	106,079
326	360,312	2,3664	-4.076	24	37	7	11	3	103,57	77,9037
327	300,783	5,1778	-4.893	21	39	2	4	3	30,96	89,543

328	316,825	4,8698	-5.464	22	44	2.25	4	3	27,05	93,36
329	220,269	1,3412	-1.453	13	22	8	7	2	120,24	47,787
330	220,269	1,3412	-1.453	13	22	8	7	2	120,24	47,787
331	296,589	3,4698	-1.443	15	29	2.5	5	1	44,48	66,5714
332	296,589	3,4698	-1.443	15	29	2.5	5	1	44,48	66,5714
333	260,38	2,3468	-2.042	16	32	6	7	1	134,44	67,8781
334	365,412	2,4606	-2.849	26	44	8.5	9	4	126,16	96,6189
335	259,304	1,7712	-2.452	19	37	4.5	5	2	74,85	74,4044
336	421,403	2,2896	-4.741	31	54	8.5	9	5	114,04	115,665
337	376,561	3,3335	-3.132	23	47	8	9	1	162,82	97,4244
338	318,409	1,0732	-0.983	22	51	5.2	7	1	99,1	88,4603
339	389,407	1,7508	-1.395	29	51	10	8	4	111,81	110,062
340	260,335	1,3183	-2.113	19	41	5.5	5	3	49,33	80,413
341	395,409	2,3615	-5.204	29	52	8.5	8	3	91,56	107,862
342	343,38	0,2127	-4.545	25	48	8	8	3	93,57	103,059
343	303,36	1,0001	-1.932	22	44	6	7	2	77,57	90,4504
344	356,422	3,0221	-3.886	24	39	7.5	8	4	126,83	92,856
345	327,404	2,5333	-4.589	23	43	6.5	7	4	101,76	90,6867
346	363,435	2,1482	-4.294	25	47	9.7	9	2	123,44	96,6574
347	304,298	2,1735	-2.154	22	39	7	7	2	103,79	76,8896
348	309,323	2,0816	-3.812	23	40	8	7	3	88,39	84,7829
349	279,335	1,5674	-2.749	20	43	6	6	3	78,51	80,4264
350	242,321	1,3401	-2.807	15	26	5	7	2	117,11	60,7967
351	337,801	2,2421	-3.5	23	44	6.5	7	2	69,72	94,8627
352	334,347	1,1089	-4.195	23	38	7.5	8	2	122,71	83,2302
353	335,643	-0,8651	-2.94	18	36	2	5	3	3,24	84,212
354	203,197	0,6736	-2.563	15	25	3.5	5	2	74,85	55,3599
355	389,919	3,446	-2.69	27	56	5	6	3	37,3	119,72
356	283,282	1,6968	-1.895	21	36	7	6	3	77,13	76,6337
357	283,241	4,6608	-2.178	15	26	2	6	1	100,47	73,6411
358	235,259	1,5026	-1.99	16	26	5	5	2	79,75	64,1345
359	376,453	3,1809	-2.869	25	43	9.5	9	3	118,32	97,5945
360	246,353	2,1008	-1.7	15	29	8	7	1	134,44	63,0711
361	325,388	2,7686	-3.861	23	40	6	7	3	98	89,5012
362	205,231	2,3076	-1.299	15	28	2.5	4	2	43,84	55,6074
363	205,231	2,3076	-1.299	15	28	2.5	4	2	43,84	55,6074
364	205,231	2,3076	-1.46	15	28	2.5	4	2	43,84	55,6074
365	205,231	2,3076	-1.46	15	28	2.5	4	2	43,84	55,6074
366	379,434	2,2801	-2.822	26	49	9.75	10	3	138,82	97,6611
367	207,724	2,42148	-2.126	12	24	3	5	0	73,48	56,5547
368	354,36	2,0514	-3.608	26	47	9.2	8	4	100,46	99,5369

369	342,338	1,9004	-2.325	22	39	8.5	11	1	92,68	71,8317
370	345,393	1,9608	-3.332	25	50	6.75	7	3	87,74	99,1024
371	423,506	3,1673	-4.996	28	50	7.5	10	2	154,71	109,986
372	379,388	2,9181	-3.155	26	44	9.25	10	2	142,21	92,8756
373	399,463	2,5708	-4.652	28	52	9	8	4	109,22	111,637
374	344,392	1,5192	-4.79	24	42	7	9	3	119,48	89,2112
375	274,341	2,0525	-1.692	19	34	5.5	6	2	85,11	74,8357
376	303,379	2,1626	-1.905	21	40	6	6	3	95,86	86,8304
377	358,392	1,4395	-3.537	26	50	7.7	8	3	103,53	102,817
378	462,524	2,7865	-2.237	33	59	10	10	5	126,59	129,38
379	444,547	3,0349	-4.793	27	42	9	12	3	195,23	108,875
380	322,361	2,519	-3.421	24	44	7	6	3	87,74	91,8414
381	331,389	2,5295	-3.492	23	42	6.75	7	3	102,02	92,5122
382	217,178	1,0693	-0.565	16	25	5	5	3	68,39	56,0192
383	395,433	0,0822	-3.639	27	50	8.75	11	3	115,12	105,841
384	335,378	2,5154	-3.137	23	42	7.5	8	3	111,78	84,5547
385	337,351	1,0631	-2.919	23	39	7.2	9	2	127,76	83,8287
386	335,421	2,365	-2.623	23	46	8	7	3	71	90,0715
387	334,37	2,1499	-3.363	24	47	7.5	8	2	114,33	92,4056
388	332,417	3,5266	-3.621	23	44	7	6	2	74,86	91,9032
389	306,704	1,7019	-3.703	21	33	7.5	8	2	94,07	74,9162
390	295,357	3,0373	-2.785	20	38	6.5	7	2	106,46	75,7237
391	274,341	2,5363	-4.35	19	34	5.25	6	2	98,14	77,7476
392	325,405	2,51728	-4.914	24	50	5.5	5	4	75,75	90,881
393	232,235	0,80328	-1.654	17	29	6.5	5	1	70,4	59,9535
394	329,307	2,167	-3.273	24	41	8	8	3	106,45	86,7939
395	321,842	4,319	-2.588	22	46	3.45	4	2	41,49	92,5815
396	281,753	4,317	-2.97	19	36	2.25	4	2	21,26	76,9187
397	327,383	0,7909	-3.643	21	35	9	10	2	152,54	78,3757
398	403,426	2,2518	-4.399	29	54	7.25	9	3	78,43	110,153
399	464,464	3,1581	-2.993	32	53	10	12	3	118,31	112,589
400	236,224	1,7624	-1.356	17	30	5.75	6	2	66,61	59,21
401	335,363	1,0226	-3.5	25	45	8.5	8	4	80,04	98,1175
402	370,49	2,3088	-1.456	24	49	10	9	4	118,84	91,759
403	376,435	4,0173	-5.493	27	47	8	8	5	107,82	101,515
404	320,364	1,4687	-3.227	22	39	7	7	2	105,64	82,8087
405	371,472	2,9834	-1.381	24	46	9.5	8	2	125,43	93,5243
406	386,508	4,0352	-3.986	27	55	8.5	6	3	74,86	111,394
407	387,499	2,7864	-5.496	27	55	8.2	8	4	97,58	109,839
408	413,493	2,6876	-3.241	29	54	8.5	9	3	122,92	111,59
409	285,298	1,9619	-3.813	21	37	7	6	2	81,18	77,0772

410	289,33	2,385	-3.718	21	41	5.5	6	2	87,24	80,6414
411	304,172	2,3899	-3.495	19	35	5	7	2	63,99	74,3157
412	331,393	1,8756	-4.516	23	42	5.5	8	3	105,42	94,6787
413	343,377	3,1994	-4.776	25	47	6.75	7	2	100,29	95,9381
414	415,443	0,9384	-4.1	30	57	9	10	3	109,38	111,74
415	276,291	0,1727	-4.582	20	37	3.5	7	2	78,15	75,5657
416	319,36	2,8505	-4.154	24	44	4.5	6	4	75,08	91,7194
417	301,32	3,1763	-3.804	21	34	6.75	7	3	119,48	76,6849
418	328,185	3,1653	-2.263	18	29	6	7	2	107,31	71,6764
419	405,476	2,3015	-3.912	29	52	8.5	9	5	108,28	118,481
420	412,482	3,2891	-5.133	30	61	4.5	8	5	117,34	110,933
421	377,436	3,3553	-4.607	28	54	8	6	4	78,51	110,243
422	353,415	2,3715	-4.452	26	52	6.5	6	4	69,72	109,241
423	360,477	3,4601	-5.448	25	52	7	8	4	102,93	98,2727
424	379,431	0,8091	-3.792	26	49	9.7	9	3	114,76	105,858
425	425,481	2,039	-3.836	31	61	10	9	4	115,47	123,043
426	384,447	2,7091	-4.227	26	51	9.75	9	2	110,39	99,9717
427	314,357	1,7662	-2.374	21	40	9.45	8	2	93,32	80,5437
428	351,401	1,3394	-3.123	23	38	8.5	9	3	139,15	88,056
429	304,367	2,2116	-3.828	21	38	7.5	7	2	102,18	81,8402
430	412,509	2,9115	-4.487	29	56	8.75	9	4	112,04	113,927
431	365,47	3,3103	-3.518	24	45	8	8	3	115,6	93,9235
432	253,298	0,9127	-2.128	18	37	6	6	1	78,51	74,5284
433	278,261	0,8884	-2.333	20	35	7.5	7	2	90,65	71,6348
434	278,261	0,8884	-2.333	20	35	7.5	7	2	90,65	71,6348
435	411,701	5,1107	-5.284	23	36	4.5	7	3	91,32	97,3748
436	435,472	2,4982	-5.189	32	61	9.5	8	5	91,14	126,703
437	351,155	0,9775	-3.061	21	34	6.5	8	3	84,3	86,3957
438	298,74	1,9186	-2.629	20	37	6	6	2	40,62	82,6575
439	298,74	1,9186	-2.629	20	37	6	6	2	40,62	82,6575
440	478,177	0,1365	-5.84	26	46	3.2	6	4	46,11	108,935
441	339,453	2,7314	-1.919	23	49	8	7	2	78,1	92,4007
442	376,409	1,4075	-4.434	28	51	8	7	4	75,51	113,104
443	310,438	2,4154	-3.457	20	39	5.5	7	2	113,35	82,5647
444	269,34	1,5268	-2.566	19	42	6	6	1	78,51	79,8094
445	325,345	3,2026	-3.196	23	37	7	8	4	108,07	83,125
446	377,415	2,632	-2.588	26	48	9.2	9	4	121,01	93,1397
447	225,311	2,068	-1.641	15	30	4.5	5	1	94,17	61,1724
448	390,316	2,1241	-4.783	28	43	6.5	10	3	95,16	93,9689
449	310,415	2,1435	-1.538	21	45	8	7	3	96,56	84,6397
450	216,163	1,9071	-1.181	15	23	4	7	2	56,21	45,6624

451	326,414	2,8474	-5.25	22	45	6	8	2	111,41	83,7957
452	290,364	2,1467	-3.079	19	31	6	7	3	113,69	76,103
453	332,381	0,4061	-3.619	23	41	7	9	3	112,9	88,485
454	391,485	3,1153	-4.225	27	54	8	8	3	123,82	110,032
455	266,276	1,352	-2.401	18	29	7.75	8	2	125,36	63,8119
456	357,404	1,7696	-4.525	26	51	7	7	3	81,5	101,897
457	438,503	1,3875	-3.928	31	57	9.5	10	5	123,26	123,443
458	443,948	4,4718	-3.805	27	44	10	11	4	164,08	105,735
459	435,545	2,4376	-4.536	31	60	8.5	9	5	105,34	126,336
460	407,419	1,9937	-4.424	30	55	7.5	8	5	96,97	113,387
461	359,463	1,9163	-1.946	26	57	8.2	6	3	61,88	107,998
462	416,476	2,4461	-4.426	31	59	8	8	5	81,67	131,599
463	236,267	1,7801	-1.605	17	33	5.75	5	1	81,42	63,2586
464	357,448	1,8828	-2.103	23	44	9.7	9	3	122,28	89,3707
465	372,441	2,9386	-5.879	26	49	6.75	8	4	111,41	96,9872
466	296,779	3,3011	-3.488	19	33	5	8	3	113,65	78,1191
467	467,412	1,4412	-1.411	32	57	7.25	13	2	119,41	111,093
468	427,921	3,9339	-3.3	28	53	8.5	9	3	80,65	106,63
469	359,443	3,0896	-3.483	25	49	8.5	7	4	80,65	95,1985
470	283,3	2,7429	-2.982	21	37	5	5	3	57,78	79,3834
471	479,434	1,2865	-3.252	34	60	8.2	12	3	170,08	114,912
472	285,341	2,3054	-3.098	21	42	6	5	3	74,85	81,8664
473	334,417	3,1541	-4.633	22	39	7	8	4	138,21	86,7027
474	448,45	3,2553	-4.776	31	53	8.75	12	3	163,25	108,497
475	360,474	2,9733	-4.826	25	51	7	7	3	95,47	104,786
476	376,369	1,6588	-3.83	28	48	8.75	9	5	102,24	104,299
477	289,31	1,7583	-1.99	20	33	7	7	3	105,37	74,5107
478	452,549	3,5902	-4.829	31	54	7.5	9	4	154,77	122,412
479	333,344	2,6341	-3.193	25	43	7.5	7	4	85,32	90,5527
480	381,382	2,388	-4.581	28	50	9	8	4	99,93	109,545
481	299,71	1,0041	-3.98	20	34	6.75	8	1	96,53	72,6811
482	258,273	0,9384	-2.236	19	35	7.2	5	3	62,4	74,9662
483	228,247	1,8112	-2.881	17	31	5	4	3	61,96	65,0649
484	298,3	0,9112	-3.11	22	39	7	8	4	91,15	85,1182
485	386,531	2,1836	-1.659	28	64	9.5	6	3	55,89	124,776
486	449,459	2,503	-5.826	33	59	9.25	10	4	122,63	127,52
487	444,478	2,3526	-4.448	32	61	5.75	9	3	116,61	125,039
488	264,3	2,1691	-2.451	18	31	4.75	6	2	99,58	66,6839
489	358,435	1,7648	-3.645	26	55	10	7	4	65,12	112,97
490	490,594	3,3905	-5.01	36	74	9.5	8	5	90,03	152,513
491	325,362	1,5671	-3.15	24	45	6	6	3	78,51	95,5794

492	264,109	1,4672	-2.382	16	27	5	7	1	63,99	62,0087
493	266,319	1,4836	-2.261	18	34	6.7	7	3	91,31	71,1537
494	266,319	1,4836	-2.261	18	34	6.7	7	3	91,31	71,1537
495	277,362	2,1591	-3.19	20	44	6	5	2	74,85	79,0994
496	394,404	3,9244	-4.403	28	46	8.5	9	5	121,6	99,155
497	291,302	1,7712	-3.461	21	39	6.75	7	2	74,61	77,1792
498	360,451	2,7541	-2.714	26	55	6.25	7	2	90,54	104,721
499	364,395	2,338	-4.237	25	43	6.5	9	2	128,43	90,3211
500	414,498	2,2582	-5.139	30	63	8.25	8	4	82,19	127,591

Figure S3 **Distribution of molecular properties of the 500 fragments.** Molecular weight (MW), LogP, LogS, number of heavy atoms (HAC), hydrogen bonds donors (HD), hydrogen bonds acceptors (HA), number of hetero atoms (nHA), number of rings (NR), polar surface area (PSA) and molar refractivity (MR).

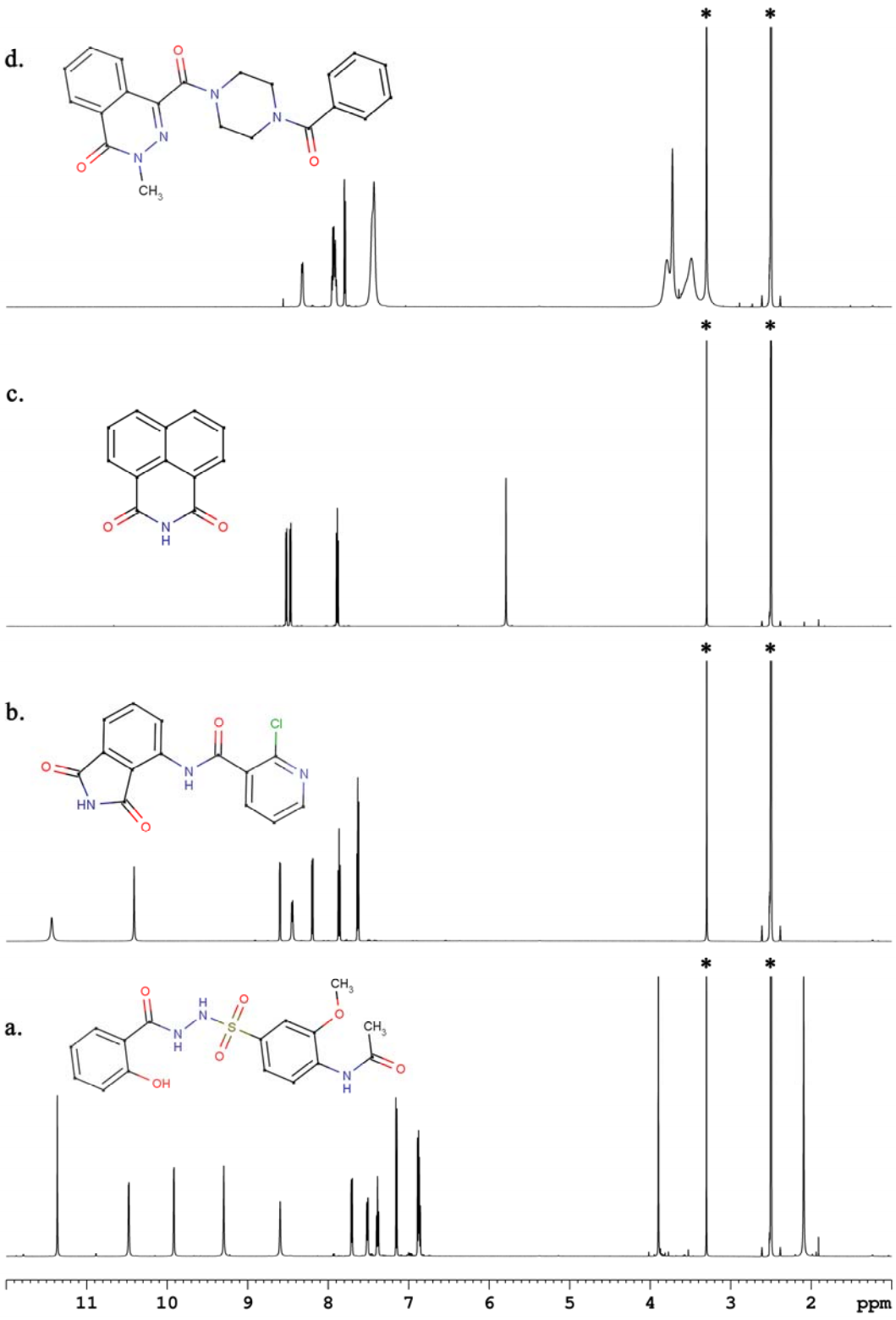
d.
c.
b.
a.
*
*
11
10
9
8
7
6
5
4
3
2
ppm

Figure S4 **NMR spectra of the best four hits**. The effects of the best hits from docking on the melting temperature T_m of the complex are shown in Fig. 8 of the paper. This figure presents the NMR spectra for a subset of the ligands that had the most pronounced effect on the complex, i.e. whose T_m varied by at least 2°C. a. NM372. b. NM156. c. NM87. d. NM442. The 1D spectra have been acquired on a Bruker spectrometer operating at the proton frequency of 600 MHz, using a cryoprobe. Asterisks denote the solvent peaks: DMSO at 2.50 ppm and the residual HDO signal at 3.30 ppm. Molecules shown in insets have been drawn with Marvin 5.11.3, 2012, ChemAxon (http://www.chemaxon.com).